Environmental Science and Ecotechnology 29 (2026) 100660

Contents lists available at ScienceDirect

Environmental Science and Ecotechnology

journal homepage: www.journals.elsevier.com/environmental-science-and-ecotechnology/

Original Research

Iron redox cycling drives enhanced methanogenesis in magnetic biochar-mediated anaerobic digestion of waste-activated sludge

Qing-Bin Meng [a,b], Zhang-Wei He [a,b,*], Zhi-Hua Li [a,b], Cong-Cong Tang [a,b], Ai-Juan Zhou [c], Bin Liang [d], Wenzong Liu [d], Yong-Xiang Ren [a,b], Aijie Wang [d,**]

[a] Key Laboratory of Northwest Water Resource, Environment and Ecology, Ministry of Education, School of Environmental and Municipal Engineering, Xi'an University of Architecture and Technology, Xi'an, 710055, China
[b] Shaanxi Key Laboratory of Environmental Engineering, Xi'an University of Architecture and Technology, Xi'an, 710055, China
[c] Department of Water Supply and Drainage, Taiyuan University of Technology, Taiyuan, 030024, China
[d] State Key Laboratory of Urban-rural Water Resource and Environment, School of Eco-Environment, Harbin Institute of Technology, Shenzhen, 518055, China

ARTICLE INFO

Article history:
Received 8 June 2025
Received in revised form
19 January 2026
Accepted 19 January 2026

Keywords:
Anaerobic digestion
Waste-activated sludge
Magnetic biochar
Iron species leaching behavior
Fe(III)/Fe(II) redox cycle

ABSTRACT

Anaerobic digestion provides an essential pathway for reducing organic waste while simultaneously recovering bioenergy. To enhance this process, magnetic biochars are frequently employed as conductive additives to promote direct interspecies electron transfer (DIET) among syntrophic microorganisms. However, the fundamental mechanisms regarding how iron species leached from these materials influence iron transformation and electron flux remain poorly understood. Here we show that the leaching of iron species from magnetic biochar establishes a stable Fe(III)/Fe(II) redox cycle that accelerates the hydrolysis, acidogenesis, and methanogenesis of waste-activated sludge. We find that cumulative methane production increases by 17% as leached Fe(III) facilitates dissimilatory iron reduction, followed by secondary mineralization into high-crystalline iron species. This process selectively enriches electroactive taxa, including *Geobacter* and *Methanothrix*, and transitioned the dominant electron transfer mechanism from cytochrome c-dependent pathways to a Fe(III)/Fe(II) redox-driven DIET. These mechanisms advance our understanding of conductive material-mediated AD, offering strategies to optimize energy recovery from waste-activated sludge and support sustainable sludge management in wastewater treatment.

1. Introduction

The activated sludge system has been extensively adopted in wastewater treatment plants (WWTPs) worldwide, playing a vital role in protecting natural water resources, ecological environment, and human health [1,2]. However, the continuous expansion and improvement of WWTPs have led to the large-scale accumulation of waste-activated sludge (WAS). The global average WAS production has been recorded at 20–40 kg per population equivalent per year [3] and is projected to exceed 127.5 million tons annually by 2030 [4]. A promising alternative to WAS treatment is anaerobic digestion (AD), which has emerged as a low-carbon footprint technology that simultaneously addresses sludge reduction and bioenergy recovery [5,6]. The recovery and use of bioenergy facilitate energy self-sufficiency in WWTPs and reduce carbon emissions from these plants [7].

Nevertheless, the low methanogenic efficiency and unstable operation of AD constrain its engineering applications. Methanogenesis refers to interspecies syntrophic metabolism, and its efficiency and rate of occurrence are affected by interspecies electron transfer (IET) [8]. Thus, recent studies have emphasized the importance of establishing direct IET (DIET) [9–11], which offers advantages in energy metabolism and electron transfer over traditional interspecies hydrogen transfer, while also presenting a

* Corresponding author. Key Laboratory of Northwest Water Resource, Environment and Ecology, Ministry of Education, School of Environmental and Municipal Engineering, Xi'an University of Architecture and Technology, Xi'an, 710055, China.
** Corresponding author.
E-mail addresses: zwhe@xauat.edu.cn (Z.-W. He), waj0578@hit.edu.cn (A. Wang).

https://doi.org/10.1016/j.ese.2026.100660

promising pathway for efficient methanogenesis. Effectively promoting DIET requires the use of exogenous conductive materials that spontaneously enrich syntrophic microorganisms [12–14]. Among such materials, biochar is favored for its functional effectiveness, environmental friendliness, and economic feasibility [15,16]. In AD, biochar can increase the resistance of methanogens to stressors via its porous framework and facilitate IET by mediating electron transfer. The problem is that biochar does not adequately promote the hydrolysis of complex organic matter (OM) [17,18]. Such hydrolysis is advanced by magnetite through the enrichment of dissimilatory iron-reducing bacteria (DIRB), but its nanoscale size and magnetic properties cause magnetite agglomeration, reducing the potential for contact among magnetite, microorganisms, and substances [19]. These challenges highlight the need to develop functional and composite conductive materials.

An example is magnetic biochar (MBC), prepared by loading nanomagnetite onto the surface of biochar; this process mitigates nanomagnetite's tendency to form agglomerates and facilitates the hydrolysis of complex OM through DIRB enrichment [14,18,20]. Meanwhile, the recoverability of MBC prevents the loss of conductive materials caused by the discharge of digested residues [14]. Despite these advantages, the iron species on MBC are typically converted to Fe(II) via dissimilatory iron reduction (DIR) in AD, accompanied by leaching into the liquid phase [18,21]. The leaching of ferrous ions facilitates the enrichment of DIRB (e.g., *Clostridium* and *Geobacter*), overcoming barriers to the hydrolysis of complex OM and advancing the redox cycling of Fe(III)/Fe(II) during AD [22,23]. These outcomes, in turn, promote the efficiency of IET between syntrophic microorganisms. Coupling iron cycling with OM degradation further accelerates methanogenesis. Importantly, from the perspective of biogeochemical iron cycling, unstable iron species are susceptible to crystalline transformation catalyzed by free Fe(II), which gradually transforms into thermodynamically more stable iron oxides [24]. The involved electron transfer can be driven by microorganisms, thus promoting OM degradation and methanation [24–27]. Although studies have demonstrated that MBC can enhance DIET between syntrophic microorganisms by mediating electron transfer and stimulating the secretion of electroactive substances, such as CytCs, in AD [20,28], most have focused on the physicochemical characteristics and microbial community enrichment in AD related to conductive materials. These works have disregarded the interaction between biological reactions and the dynamic behavior of the iron species leached from MBC.

The iron species leached from MBC may mediate DIET by forming an electron storage system linked to iron redox cycling. In this process, syntrophic acetogens and methanogens may cooperate to facilitate electron transfer driven by the iron redox cycle, thereby enhancing OM oxidation, acetate degradation, and methanation. DIET facilitated by exogenous iron oxides may also involve coupling Fe(III)/Fe(II) redox cycling with secondary mineralization [29]. Notwithstanding these potential functions, however, few studies have shed light on the fate of iron contained in MBC during AD. In particular, nothing is currently known about the effect of iron redox cycling that involves the iron species leached from MBC on AD.

To address the aforementioned deficiencies, the present study explored how iron species leached from MBC affect AD and the role of iron redox cycling in this process. We first examined the influence of MBC on AD efficiency, then investigated the migration and transformation patterns of leached iron species in both solid and liquid phases. We also evaluated the leaching of iron species from MBC-mediated methanation to uncover the mechanism by which these species enhance or strengthen methanation. Finally, we comprehensively delineated the transformation of the iron species leached from MBC during AD. By illuminating the migration and transformation patterns of such species and the potential mechanisms mediating IET, this study provided new insights into both the theorization and the application of MBC-mediated DIET to enhance methanogenesis. These endeavors are expected to stable sludge management in industrial AD systems and support policy making for sustainable sludge disposal.

2. Materials and methods

2.1. Characteristics of WAS, seed sludge, and MBC

Waste-activated sludge was sourced from a secondary sedimentation tank in a WWTP located in Xi'an, China. Thermal pretreatment is widely used to promote sludge solubilization, so we treated the WAS at 80 °C for 30 min [14,20,30] to obtain a substrate. Seed sludge was obtained from a laboratory-scale, semi-continuous anaerobic digester fed with pretreated WAS. The digester had a working volume of 500 mL and was operated with daily feedings and discharges of 30 mL of WAS. The typical characteristics of the seed sludge are presented in Supplementary Table S1.

Raw biochar was obtained from Xuchang Environmental Protection Industry Co., Ltd., China. It was produced by pyrolyzing fruit wood at 500 °C for 2 h under nitrogen, then ground to a powder with particle sizes of 0.3–0.9 mm. MBC was prepared via co-precipitation (Supplementary Text S1 [20]), and the properties of both types of biochars are listed in Supplementary Table S2.

2.2. AD experiment design and operation

2.2.1. Methanation

Experiments were carried out in anaerobic digesters with a working volume of 90 mL, fed with 81 mL of pretreated sludge and 9 mL of inoculum [31]. To evaluate the roles of MBC in AD for methanation, we prepared three samples: WAS with no additives (control, R1), WAS mixed with biochar (R2), and WAS incorporated with MBC (R3). Following previous studies, 8 g L^{-1} of the biochar and MBC were added to samples R2 and R3, respectively [16,32,33]. High-purity nitrogen gas was flushed into the digesters to remove oxygen before the WAS samples were incubated in a water bath shaker at 35 ± 1 °C and 105 rpm. This experiment was designed to measure biogas, which was collected using a gas sampling bag (MBT11, HEDE, China). All the experiments were conducted in triplicate.

2.2.2. Physicochemical indicators

Batch experiments were carried out under the same conditions and with the same sample groups as those described in Section 2.2.1. These experiments were intended to identify the physicochemical characteristics of AD influenced by the aforementioned additives and to determine the distribution of iron ions between the solid and liquid phases. All solid phases used in this work are sludge phases separated from either biochar or MBC using a 100-mesh screen. To prevent excessive gas pressure from damaging the digesters, biogas was collected into a gas sampling bag. These experiments were also performed in triplicate.

2.2.3. Fates and effects of iron species leached from MBC

To investigate the interaction between the dynamic behaviors of the iron species leached from MBC and the biological reactions occurring during AD, batch experiments were conducted under the same conditions and groupings as those described in Section 2.2.1. Destructive sampling was adopted, with the endpoints of

three typical AD stages serving as the time points. Specifically, we set up nine reactors, three for each sample group (R1–R3) corresponding to three destructive sampling time points at the end of the hydrolysis stage (Day 5), at the end of acidogenesis (Day 20), and at the end of methanogenesis (Day 30) [34,35]. The sludge samples obtained from each experimental group were used to characterize the composition of iron species and the structure of microbial communities in suspension. The biochar and MBC obtained in each group were used to analyze the leaching behavior of iron species and the structure of the microbial communities in the biofilm. The electrochemical properties of AD were also characterized, and all experiments were performed in triplicate.

2.3. Chemical analysis

Before physicochemical analysis, the sludge samples were centrifuged at 8000 rpm for 10 min, then filtered through a 0.45 μm membrane. Total suspended solids, volatile suspended solids (VSS), and chemical oxygen demand (COD) were tested using standard methods [32], while pH, proteins, polysaccharides, and short-chain fatty acids (SCFAs) were assessed in accordance with previously published descriptions [14] (Supplementary Text S2). Biogas composition and quantity were examined using a gas chromatograph (GC9720 Plus, Fuli, China) equipped with a thermal conductivity detector. The output pressures of the hydrogen and air generators were 0.3–0.5 MPa.

2.4. Identification and detection of iron species leached from MBC

A modified 1,10-phenanthroline method was employed to quantify the Fe(II) and total iron concentrations in the liquid phase. The Fe(III) concentration was then calculated as the difference between the total iron and Fe(II) contents. The method employed here was described in a previous study [36]. The iron species in the solid phase were identified using a sequential extraction technique [37,38] described in Supplementary Text S3.

2.5. Electrochemical analysis of anaerobic sludge

Electrochemical analyses were performed using an electrochemical workstation (Zhenhua 660F, China). Before testing, the sludge samples were centrifuged at 8000 rpm for 10 min and rinsed three times using 0.1 mol L^{-1} NaCl solution. Redox capacity and the electrical conductivity of anaerobic sludge were examined by cyclic voltammetry (CV) and electrochemical impedance spectroscopy (EIS) [39] (Supplementary Text S4).

2.6. Identification of iron species in sludge and MBC

We used X-ray diffraction (XRD) to identify crystalline iron phases in sludge samples and MBC collected at each destructive sampling time ($2\theta = 10–80^\circ$; step size: 0.02°, scan rate: 5° min^{-1}). Raw XRD curves were retrieved and compared in Jade 6 software. X-ray photoelectron spectroscopy (XPS) was conducted to characterize changes in elemental states of the iron species in the sludge samples and MBC at the destructive sampling times. The XPS curves of Fe 2p were peak-fitted using Avantage software, and all spectra were calibrated using the standard C 1s peak at 284.8 eV. After fitting, the area percentages of Fe(III) and Fe(II) were determined. All sludge samples were processed by vacuum freeze-drying before characterization. To characterize the MBC samples, they were treated with ultrasound for 10 min and rinsed three times with deionized water to remove biofilm from their surfaces.

2.7. Microbial community activities and the evolution of microbial community structures

Sludge samples, including both suspension and biofilm, were collected on days 5, 20, and 30 to track changes in bacterial and archaeal communities under the iron species leached from MBC. Primers 338F and 806R were used to detect bacteria in the samples, and primers 524F10extF and Arch958RmodR were employed to identify archaea. Microbial functional prediction was performed using the PICRUSt tool on the Majorbio Cloud platform, followed by visualization of the predicted pathway profiles using TBtools-II. Microbial communities were characterized, and the data were analyzed primarily using R software (version 4.3.2). Bubble plots and Sankey stacked diagrams were created using the *ggplot2* package (v3.2) [40].

Protease and α-glucosidase activities (Geruisi, China), as well as coenzyme F420 and c-type cytochromes (CytCs) (Herbal Source, China), were quantified using commercially available assay kits. The electron transport system (ETS) was determined through the INT (2-(4-iodophenyl)-3-(4-nitrophenyl)-5-phenyltetrazolium chloride)–ETS method [41].

2.8. Calculation methods

Short-chain fatty acids used in this study included acetate, propionate, iso(n)-butyrate, and iso(n)-valerate. COD conversion factors for representative organic substrates were taken from a previous study [42].

The modified Gompertz model was used to estimate the maximum methane production rate and lag phase [43] (equation (1)).

$$P = P_m \times \exp\left\{ -\exp\left[\frac{R_m \times e}{P_0}(\lambda - t) + 1\right]\right\} \quad (1)$$

where all the variables are consistent with the definitions described in a previous study [14].

The degradation of soluble polysaccharides and proteins was evaluated using modified pseudo-first-order and pseudo-second-order kinetic models [44], represented by equations (2) and (3), respectively:

$$Q_t = Q_e\left(1 - e^{(-K_1 t)}\right) \quad (2)$$

$$Q_t = \frac{K_2 Q_e t}{1 + K_2 Q_e t} \quad (3)$$

where Q_e is the largest degradation capacity (mg COD L^{-1}) at the termination of reaction, Q_t is the degradation capacity (mg COD L^{-1}) at time t (days), and K_1 and K_2 are the pseudo-first- and pseudo-second-order rate constants, respectively.

The specific capacitance (C_p) of sludge was calculated by integrating the area of the CV curve into the computation [45]:

$$C_p = \frac{A}{2mk(V_2 - V_1)} \quad (4)$$

where C_p denotes the specific capacitance (F g^{-1}), A is the area within the CV curve (AV), V_1 is scanned at low potential (V), V_2 is scanned at high potential (V), m represents the mass of dry sludge (g), and k is the scan rate (mV s^{-1}).

Statistical analyses were performed via a t-test, with $P < 0.05$ considered statistically significant. Correlation analyses were conducted using the ggcor package and visualized via https://www.chiplot.online/ [46].

3. Results and discussion

3.1. AD performance

3.1.1. Methane production

The additive induced a significant improvement in AD performance (Fig. 1). Cumulative methane production increased by 3.8% and 17.0% in R2 and R3, respectively, over the levels observed in R1 (Fig. 1a). Specifically, methane production in R3 was the highest, with the sample exhibiting a maximum cumulative methane production of 305.3 ± 5.6 mL per g VSS. Although maximum methanogenesis occurred on Day 10 in all samples, R3 showed a significant increase in this activity (Fig. 1b). The modified Gompertz model fit the experimental data well, with R^2 values of 0.998, 0.998, and 0.997 for R1, R2, and R3, respectively (Supplementary Table S3). The results presented a remarkably elevated maximum methane production potential (P_m) for R3, suggesting superior substrate bioconversion in the sample. Notably, although R2 and R3 exhibited advantages in terms of reductions in methanogenic lag time (λ), the kinetic promotion effect of R3 on R_m was markedly greater than that of R2. These findings point to the noticeable favorable effects of MBC on AD.

3.1.2. Conversion of intermediate metabolites

The conversion of intermediate metabolites is crucial for methanogenesis during AD [47]. In this study, the effects of MBC on hydrolysis were assessed based on soluble proteins and polysaccharides (Fig. 1c and d). Compared with R1, R2 and R3 exhibited a rapid decrease in soluble protein concentration, which may be attributed to the dual effects of biochar-mediated microbial activity and adsorption behavior [16]. As the reaction progressed, the effects of soluble protein consumption in R2 and R3 continued to demonstrate a significant advantage (Fig. 1c). Specifically, soluble protein concentrations rapidly decreased to 126, 26, and 11 mg COD L^{-1} in R1, R2, and R3, respectively. This phenomenon may be attributed to two factors. First, the binding of MBC-associated Fe(III) and Fe(II) to proteins via hydrogen bonding was critical in promoting subsequent protein hydrolysis [18]. Second, the iron species leached from MBC stimulated the DIR process, which in turn facilitated OM conversion [43]. The soluble protein concentration increased slightly in R1 on Day 7 (Fig. 1c), possibly because soluble protein solubilization is more efficient than hydrolysis at this stage. This finding further illustrated that MBC promoted the use of soluble proteins by the microorganisms in the sample, accompanied by increased protein hydrolysis. In contrast with the soluble protein concentrations, the concentrations of soluble polysaccharides in each group decreased sharply on Day 1 (Fig. 1d), which is attributed to the fact that polysaccharides are more easily used by microorganisms [20]. Subsequently, polysaccharide concentrations plateaued until the end of AD, with the lowest content observed in R3, indicating adequate polysaccharide consumption [14].

The kinetic fitting curves of soluble proteins and polysaccharides are presented in Supplementary Fig. S1. In terms of R^2, the pseudo-second-order kinetic model was more suitable for describing changes in soluble polysaccharides and proteins in AD under MBC treatment. The largest degradation (Q_e) of polysaccharides at the termination of reaction was exhibited by R3, reaching 138 ± 3 mg COD L^{-1}, which kinetically confirmed the promotive effect of MBC on polysaccharide degradation. Although the largest degradation of proteins in R1 was higher than that in R2 and R3 (Supplementary Fig. S1a–c), the slope of the fitted curves was lowest in R1, suggesting that this sample required more time to reach the most extensive degradation capacity, and implying an increased lag time during the degradation of soluble proteins. This result is similar to the methanogenic lag time observed in R1

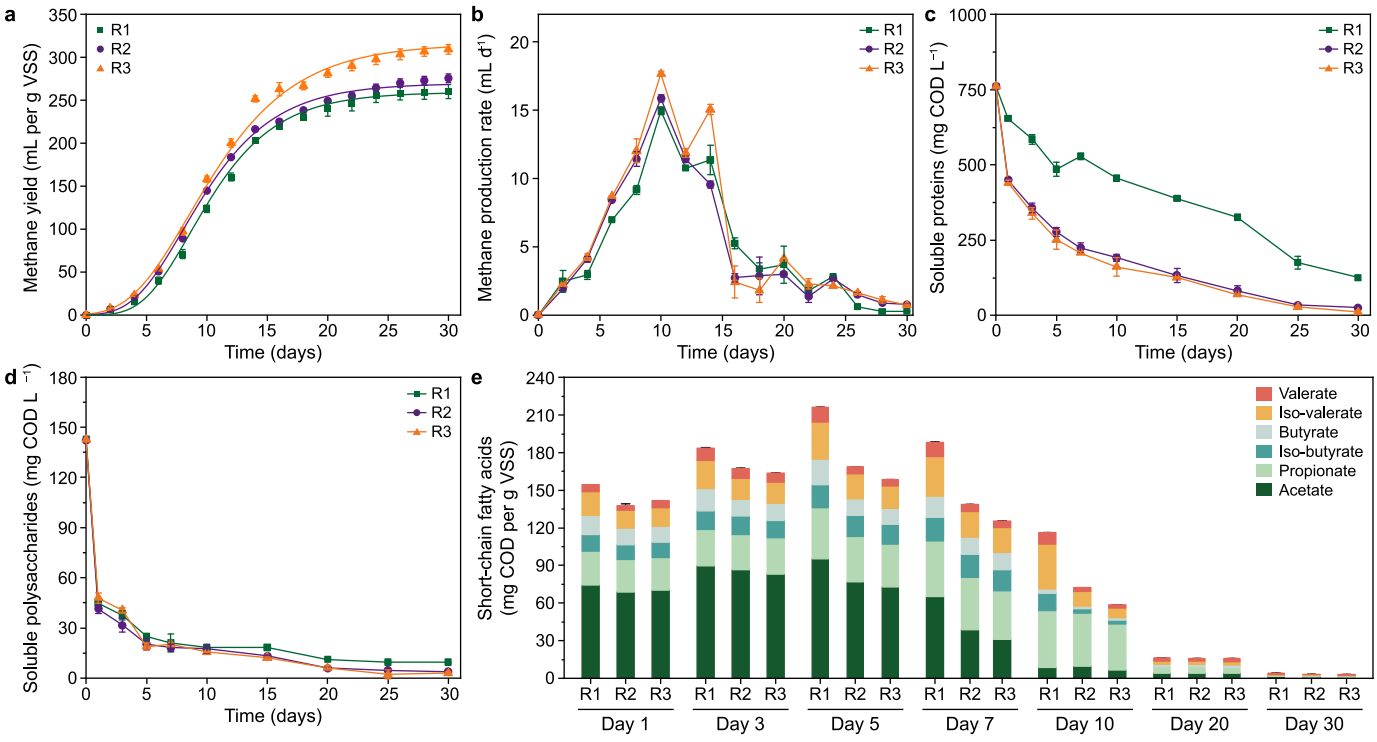

Fig. 1. Performance of anaerobic digestion affected by different additives: cumulative methane production (**a**), methane production rate (**b**), soluble proteins (**c**), soluble polysaccharides (**d**), and short-chain fatty acids (**e**). VSS: volatile suspended solids (VSS), COD: chemical oxygen demand. R1: control group, R2: biochar group, and R3: magnetic biochar group.

(Supplementary Table S3). In addition, the degradation of proteins in R3 yielded the highest R^2, indicating that MBC plays a dominant role in improving the efficiency of protein degradation.

3.1.3. SCFAs conversion

Variations in components of SCFAs were identified (Fig. 1e). The production and consumption of SCFAs are dynamic in AD. Fermentative bacteria promote SCFAs accumulation by degrading OM, while methanogens accelerate SCFAs consumption via methane production [39]. In this research, SCFAs accumulation was considerably lower in R2 and R3 than in R1 by Day 10 ($P < 0.05$). Notably, both biochar and MBC facilitated OM-to-SCFAs conversion. This enhancement is likely due to biochar and MBC serving as conductive carriers that establish DIET between microorganisms [14] while simultaneously facilitating biofilm formation and promoting mass transfer [48]. SCFAs accumulation declined from Day 7 in R1 and from Day 5 in R2 and R3, with a more pronounced downward trend observed in R3. These results indicate that MBC exerts a strong positive effect on SCFAs metabolism. Additionally, MBC provided a suitable pH environment for subsequent methanogenesis by promoting SCFAs metabolism (Supplementary Fig. S2) [49].

For individual SCFAs (Supplementary Fig. S3), acetate and propionate prevailed in the acidogenesis stage. Acetate was degraded the fastest in R3, with concentrations 46.8% and 25.6% lower than in R1 and R2, respectively, on Day 7, indicating that MBC accelerated acetate consumption. This phenomenon can be ascribed to two possible factors: First, MBC functions as an electron-transfer mediator, thereby forming an electrical network among syntrophic microorganisms [14]. Second, the iron species leached from MBC accelerate electron transfer between syntrophic microorganisms by stimulating iron redox reactions [29]. Furthermore, propionate was the dominant SCFAs after Day 10. As propionate requires dramatically higher Gibbs free energy to metabolize than other SCFAs, it is often a persistent problem in AD [17,50]. Nonetheless, the propionate in this study was metabolized faster in R3 than in the other two sample groups. This result is similarly attributable to two aspects: To begin with, the synergistic effect of biochar and magnetite in MBC promotes the conversion of SCFAs into acetate [6]. Moreover, the iron redox reactions mediated by the iron species leached from MBC alleviate the thermodynamic constraints imposed on the conversion of complex OM, such as propionate, by providing abundant electron fluxes [51]. Overall, MBC was more conducive to the conversion of intermediate products for methane production in AD.

3.2. Transfer and transformation properties of iron species in MBC

3.2.1. Distribution of iron species in the liquid phase

Magnetic biochar not only acts as a conductive carrier but also functions as a “micro-electrolysis system” by releasing Fe(III) and Fe(II) to further elevate IET efficiency [20,43]. During the hydrolysis stage, the Fe(II) concentrations in the liquid phase of all the sample groups were typified by various increasing trends (Fig. 2a). This might be attributed to the decrease in pH of AD related to the OM-to-SCFAs conversion (Fig. 1c and d; Supplementary Fig. S2). Specifically, Fe(III) tends to be converted into Fe(II) in its dissolved state under acidic conditions, while Fe(II) is essential for hydrolase secretion from microorganisms [52,53]. During acidogenesis and methanogenesis, the Fe(II) concentrations in the liquid phases of R1 and R2 remained almost stable, whereas the MBC consistently increased the Fe(II) concentration to 171.9 mg L^{-1} on Day 30. This value is considerably higher than those observed in R1 and R2 (Fig. 2a). This sustained increase is attributed to the continuous leaching of Fe(III) species from MBC, which serve as electron acceptors for the degradation of SCFAs. The elevated Fe(II) levels may have promoted the conversion of other SCFAs into acetate, thereby increasing Fe(II) accumulation and enhancing the DIR process (Fig. 1e).

Furthermore, the Fe(III) concentrations in the liquid phase of R3 fluctuated (Fig. 2a). This result could have stemmed from the metabolic processes of the microorganisms that stimulate the release of Fe(III), an exchangeable iron in the solid phase, into the liquid phase, which is subsequently converted into Fe(II) as redox reactions are triggered. For example, substances such as humic acids in extracellular polymeric substances (EPSs) present in sludge [14] contain active functional groups that can form complexes with Fe(III) [54]. Phospholipids in cell walls may also provide binding sites for Fe(III) [55], which can generate abundant iron oxides in organic-bound form. Accordingly, the Fe(III) in the solid phase was transferred to the liquid phase upon cellular rupture and substance consumption in EPSs. This enabled the bioavailability of Fe(III). These results were confirmed by subsequent analysis of iron species. Notably, the Fe(III) content in the liquid phase of R3 was significantly elevated relative to that in R1 and R2, peaking on Day 10 (Fig. 2a) and corresponding to the maximum methanogenic rate. This suggests that the iron species in MBC first leach into the liquid phase as Fe(III) to drive DIR [55], which, in turn, enriches the liquid phase with Fe(II), confirming variations in Fe(II) concentration in the liquid phase. This also confirms that the iron species leaching from MBC facilitates methanation.

We further elucidated the transformation and distribution of iron in MBC and the solid phase at different AD stages related to the iron species leached from MBC (Fig. 2b and c). In the Fe 2p short scans of MBC at different reaction periods, the deconvoluted Fe $2p_{3/2}$ spectra were Fe(II), Fe(III), Fe(II) satellite, and Fe(III) satellite [56]. The iron valence distribution showed that the original MBC possessed an elevated Fe(III)/Fe(II) ratio (Fig. 2b), consistent with a study reporting that the iron species in MBC are present primarily in Fe(III) [20]. Notably, the Fe(III)/Fe(II) ratio in MBC gradually decreased and stabilized after hydrolysis and acidogenesis, suggesting that Fe(III) is the substance predominantly leaching from MBC (Fig. 2b). The iron species that could have leached from MBC into the solid phase was Fe(III), but such species in the solid phase of R3 gradually decreased during hydrolysis and acidogenesis (Fig. 2c). These results imply that the iron species from MBC initially leached into the liquid phase as Fe(III). Subsequently, Fe(III) in the liquid phase provides sufficient Fe(II) through DIR [55], and the accumulated Fe(II) adsorbed by the solid phase contributes to the reduction of Fe(III). Interestingly, the proportion of Fe(III) in the solid phase of R3 exhibited an elevated trend during methanogenesis (Fig. 2c). Therefore, the Fe(II) adsorbed by the solid phase further stimulated the secondary mineralization of Fe(III) in the solid phase [24,29]. Hence, during the hydrolysis and acidogenesis stages, the Fe(III) leaching from MBC into the liquid phase increased the degradation of intermediate metabolites and SCFAs by stimulating DIR [38]. This was accompanied by an elevated Fe(II) concentration in the liquid phase. During subsequent methanogenesis, the Fe(II) in the liquid phase was adsorbed and electronically exchanged by Fe(III) in the solid phase, and Fe(III) exhibited superior thermodynamic stability.

3.2.2. Compositions and changes in iron species in the solid phase

To further evaluate the effects of MBC on the dynamics of iron species in the solid phase, a sequential extraction method was used to analyze the composition of iron species in sludge samples collected at different AD stages. The results showed that the iron species in raw sludge were dominated by organic-bound, exchangeable, and easily reducible states, accounting for 71.3%,

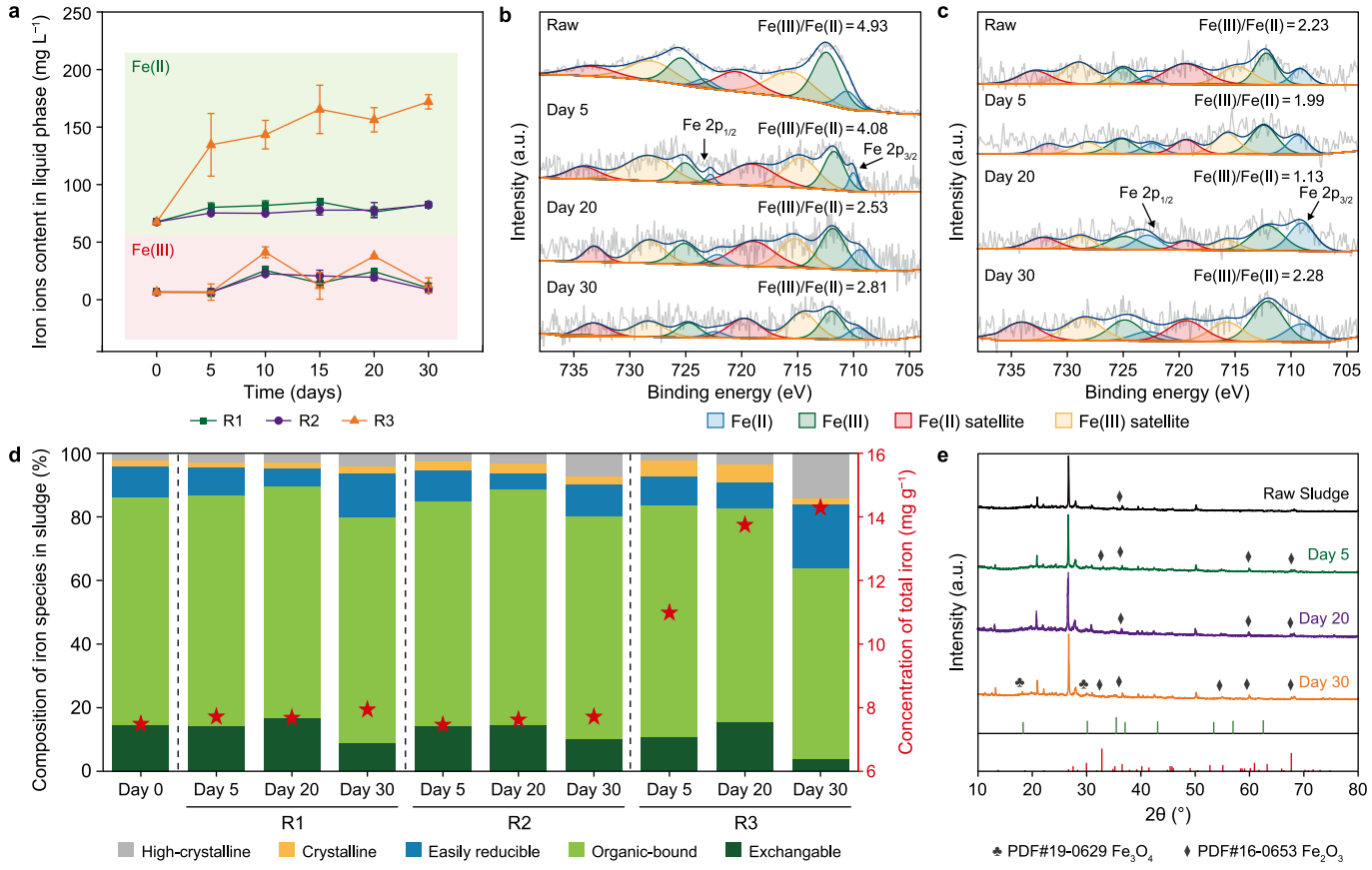

Fig. 2. **a**, The distribution of iron ions in the liquid phase: the content of Fe(III) and Fe(II). **b**–**c**, X-ray photoelectron spectroscopy Fe 2p spectra of magnetic biochar (MBC, **b**) and sludge (**c**) in R3 during different stages in anaerobic digestion. **d**–**e**, Changes in iron species: composition of iron species in sludge and total iron concentration (**d**) and X-ray diffraction patterns of sludge in R3 (**e**). The star symbols in panel **d** represent the total iron concentration. R1: control group, R2: biochar group, and R3: MBC group.

14.8%, and 9.8% of the total iron, respectively (Fig. 2d). Organic-bound iron species are composed of Fe(III), Fe(II) produced by DIR, and dissolved organics [57]. The WAS was subjected to thermal pretreatment, which could drive the release of OM complexed with iron species, thereby increasing the organic-bound iron state [55,58]. The total iron in R3 increased gradually compared with that in R1 and R2, so the iron species leached from MBC supported the increase in Fe(III) concentration in the solid phase. Notably, R3 showed a remarkable decrease in organic-bound iron species from 71.3% on Day 0–65.6% on Day 30 (Fig. 2d). The hydrolysis and acidogenesis of OM were strongly and negatively correlated with the concentrations of organic-bound iron species [55]. Therefore, during these stages, the OM conversion promoted the release of organic-bound iron species, which then induced the transition of iron species. More importantly, during the methanogenesis stage, the percentage of high-crystalline iron species in R3 increased significantly from 2.2% to 15.4% with the leaching of iron species from MBC. This study demonstrated that the degree of crystallinity in iron species increased with increasing Fe(II) dosage, typically accompanied by a closed-loop Fe(III)/Fe(II) redox cycle [29,38,59]. Notably, the XRD results similarly indicated that high-crystalline iron species were detected in the solid phase of R3 as the reaction progressed (Fig. 2e). Therefore, Fe(III) leached from MBC facilitates the secondary mineralization of iron species in the solid phase, leading to the accumulation of high-crystalline iron species.

With respect to the fates and effects of the iron species contained in MBC in the AD period, the Fe(III) leached from MBC facilitated the conversion of intermediates by accepting the electrons released from OM oxidation, after which the species was reduced to Fe(II) during hydrolysis and acidogenesis [38]. The abundance of Fe(II) provided sufficient reductive power for methanogens to catalyze CO_2 reduction, contributing to the improvement of DIET efficiency. Subsequently, the accumulated Fe(II) mediated the secondary mineralization of unstable Fe(III) during methanogenesis, which might have served as the electron acceptors for acetogens [29]. Although magnetite, as the end product, was not favorable for sustaining the iron redox cycle, it functioned as a conductive material that facilitated DIET between syntrophic acetogens and methanogens.

3.3. Electrochemical indicators stimulated by MBC

Magnetic biochar mediates DIET by closely interacting with microorganisms, which regulate redox activity and electron transfer capacity during AD [14,20]. The CV curves of the sludge samples are shown in Fig. 3a. Compared with the RV curve of R1, those of R2 and R3 exhibited higher oxidation peak potentials of 1.92 and 1.98 mA, respectively, with no significant differences found between the latter two ($P > 0.05$). Specifically, the sludge sample from R3 exhibited a greater peak reduction potential (−1.73 mA), indicating improved electrochemical activity [60]. These results indicate that the production of highly active redox species can be promoted by biochar, and that reductive activity can be enhanced by MBC-mediated Fe(II) enrichment, further stimulating IET. Furthermore, the C_p of samples can be expressed by the integral area of the CV curve [61]. The C_p of the sample in R3

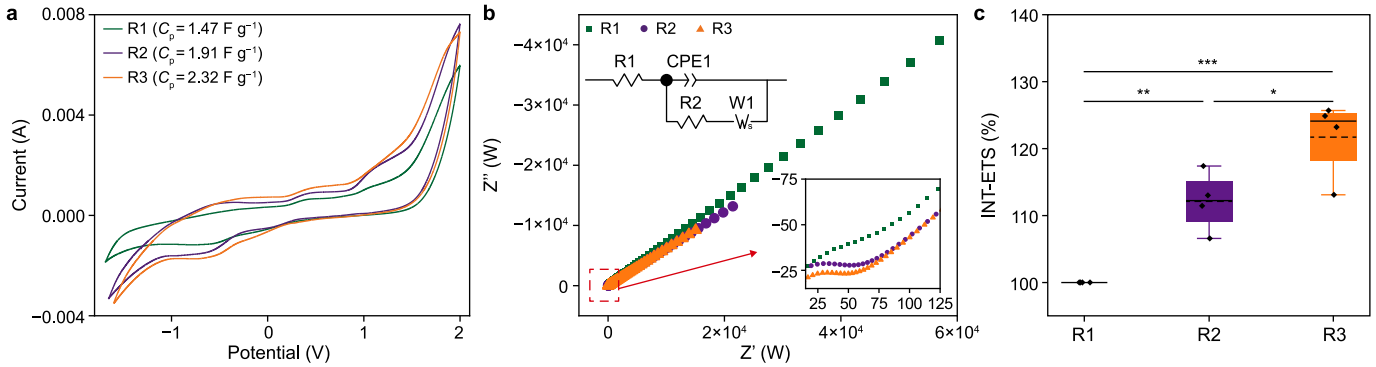

Fig. 3. Electron transfer properties of sludge in different experimental groups: cyclic voltammetry (**a**), electrochemical impedance spectroscopy (**b**), iodonitrotetrazolium chloride–electron transport system (INT–ETS, **c**). For panel **b**, the electrical equivalent circuit is shown alongside a magnified view of the high-frequency region. For panel **c**, box plots show the median (center line), mean (dashed line), and individual measurements (points); *$P < 0.05$, **$P < 0.01$, ***$P < 0.001$. R1: control group, R2: biochar group, and R3: magnetic biochar group.

increased by 57.8% and 21.5% over the values observed in R1 and R2, respectively, which indicated that the iron species leached from MBC increased the charging and discharging of anaerobic sludge (Fig. 3a). The charging and discharging of samples are determined by the redox-active substances secreted by microorganisms during AD [62,63]. Thus, MBC can amplify the accumulation of redox-active substances, which can function as electron shuttles that enhance IET in microorganisms.

Electrochemical impedance spectroscopy provides insights into frequency properties and equivalent resistance [64]. Different samples exhibited distinct Nyquist curves (Fig. 3b). At high frequencies, the arc diameter reflects the electron transfer resistance (Ret), which governs electron transfer at the electrode interface. At low frequencies, the ideal Nyquist plot forms a straight line perpendicular to the *x*-axis, demonstrating an ideal supercapacitor that is free from ion diffusion restrictions [12]. A narrower arc diameter observed in R3 indicated a lower electron-transfer resistance. The Ret parameters were fitted by establishing equivalent circuit diagrams. The results showed that R3 had a lower Ret (33.3 Ω), which was reduced by 29.2% and 20.7% compared with R1 and R2, respectively (Supplementary Table S4). The electron transfer mediated by DIR can elevate the conductivity of sludge samples [65], and the iron species leached from MBC may improve IET between microorganisms by enriching DIRB with conductive pili. In addition, an iodonitrotetrazolium chloride–electron transport system (INT–ETS) is an important indicator for assessing microbial electron transfer activity [6,41]. The activity of INT–ETS was elevated in R3 by 21.7% and 10.0% relative to that in R1 and R2, respectively (Fig. 3c). This occurrence can be attributed to the fact that the iron species leached from MBC enhance IET by increasing capacitance and electron transfer, consistent with methanogenic efficiency (Fig. 1a).

3.4. Identification of microorganisms responding to iron redox cycling

3.4.1. Activities of microorganisms

The activities of microorganisms, essential indicators in evaluating the metabolism level associated with AD performance (Fig. 4). On Day 1, the activity of protease in R1 was slightly higher than that in R2 ($P < 0.05$) but similar to that in R3 ($P > 0.05$) (Fig. 4a). The concentrations of soluble proteins in R2 and R3 were lower than those in R1 (Fig. 1c), confirming that biochar adsorption was critical to the decrease in soluble protein concentrations at the beginning of AD compared with the enhancement of microbial activity mediated by biochar. On Day 5, R3 showed considerable protease activity, consistent with the changes in soluble protein concentrations. Furthermore, the α-glucosidase activity in R3 was superior to that in R2 and R3 throughout the hydrolysis stage (Fig. 4b). Although some studies attributed the enhancement of hydrolase activity to the iron species in MBC [18,20], the current work found that hydrolase activity gradually improved with the leaching of iron species (Fig. 4a and b). This was confirmed by the subsequent correlation analysis (Fig. 7; Supplementary Fig. S5). Therefore, the iron species leached from MBC stimulate enzyme synthesis or induce enzyme gene expression via microelement supply (e.g., iron ions) while improving the efficiency of hydrolase secretion by enriching hydrolytic bacteria [18]. These outcomes subsequently accelerate the degradation of soluble OM [18].

Coenzyme F420, which is instrumental in the CO_2 reduction pathway of methanogenesis, assists in the transformation of methane precursors [47]. Its activity peaked on Day 10 in all the sample groups (Fig. 4c), in line with the maximum methane production rate (Fig. 1a). The activities of coenzyme F420 in R3 increased by 21.8% and 21.1% over the levels observed in R1 and R2, respectively, indicating that methanogenesis via the CO_2 reduction pathway was upregulated.

CytCs are vital to the respiratory electron transport chain in the cell membrane [62]. CytC dynamics are presented in Fig. 4d. Similar to coenzyme F420, CytCs were highest in R3 and peaked on Day 10, demonstrating that MBC significantly stimulated CytC secretion. An increased level of CytCs suggests that more electron mediators participate in extracellular electron transfer [15]. Nevertheless, the CytC levels in R3 were significantly lower than those in R1 and R2 on Day 20. This reduction may be attributed to the iron species leaching from MBC, in which case, both the concentration and composition of iron species change, gradually becoming more thermodynamically stable. However, CytCs are not a necessary factor for DIET in the presence of iron species represented by magnetite [29].

3.4.2. Principal component analysis of microbial communities

The bacterial communities in the suspension of R3 were separated from those in R1 and R2 (Supplementary Fig. S4a). The bacterial communities in the biofilm of R3 exhibited a more pronounced tendency toward directional succession, reflecting a consistent shift in microbial community structure toward a more functionally stable and specialized state [34]. Furthermore, the directed succession of microbial community structures contribute to the operational stability of an AD system [66]. Our results

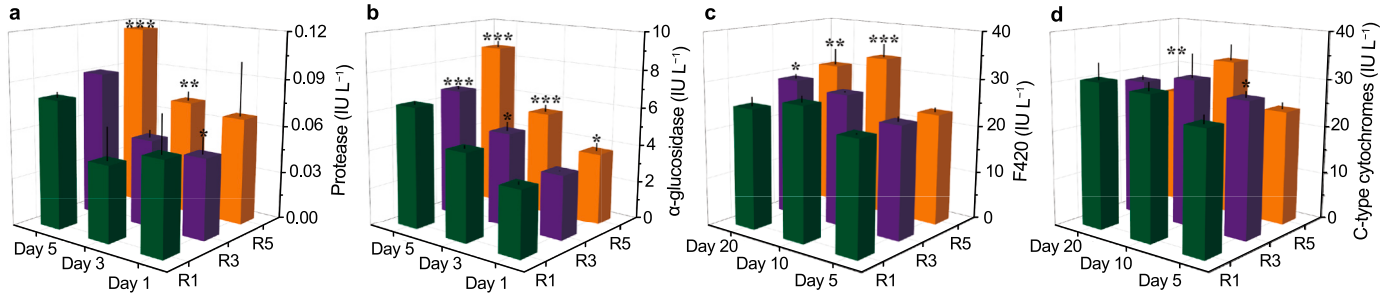

Fig. 4. The activity changes of key enzymes: protease (**a**), α-glucosidase (**b**), coenzyme F420 (**c**), and C-type cytochromes (**d**). *$P < 0.05$, **$P < 0.01$, and ***$P < 0.001$. R1: control group, R2: biochar group, and R3: magnetic biochar group.

suggest that MBC dominates the enrichment of functional microorganisms, thereby achieving the directional succession of bacterial community structures in biofilms. Meanwhile, the iron species leached from MBC increases the abundance in suspension. Furthermore, in our work, MBC exerted pronounced effects on archaeal communities (Supplementary Fig. S4b). In suspension, although the archaeal communities across the three sample groups exhibited significant variability, R3 showed a stronger tendency toward directional succession. In terms of temporal succession, the archaeal communities in R2 gradually shifted from dissimilarity to similarity, but they remained consistently different in R3. Thus, the iron species leached from MBC exerted a remarkable effect on the archaeal communities between the biofilm and the suspension.

3.4.3. Structures of microbial communities in suspension

Firmicutes, Bacteroidota, and Chloroflexota, as typical and functional phyla in AD, were highly abundant in the suspension of all the sample groups, with total percentages exceeding 70.0% (Fig. 5a). Firmicutes, widely known for their fermentative capabilities [14], dominated the microbial communities across all the groups, particularly in R3, consistent with the enhanced hydrolysis and acidogenesis (Fig. 1c–e). The relative abundance of Chloroflexota in R3 reached 12.7% at the hydrolysis stage compared with 9.1% and 8.1% in R1 and R2, respectively. Chloroflexota is considered a potential DIET-capable bacterium in AD, which not only contributes to the conversion of macromolecules into SCFAs but can also indirectly participate in the reduction of Fe(III) via the electrons generated by fermentative bacteria [67]. At the genus level, *Macellibacteroides*, *Romboutsia*, and *Clostridium* were predominant in all the groups during hydrolysis, while the predominant genera gradually shifted to *Romboutsia*, norank_f__*Bacteroidetes*_vadinHA17, *Clostridium*, and *Blvii28_wastewater-sludge_group* with changes in the substrate and physicochemical properties of AD (Fig. 5b). Among them, the typically electroactive bacteria *Clostridium* and norank_f__*Bacteroidetes*_vadinHA17 were significantly enriched in R2 and R3. This agrees with previous studies indicating that biochar and MBC can enrich potential electroactive bacteria and stimulate DIET with methanogens [20,68]. Of note was the increase in the abundance of the dominant genus *Romboutsia* (Firmicutes) from 11.7% to 17.3% in R3. In contrast, this genus proliferated to 13.3% and 15.4% in R1 and R2, respectively. *Romboutsia* is recognized as DIRB, capable of degrading complex OM and transferring extracellular electrons to insoluble Fe(III) oxides via type IV pili [69]. The findings suggest that the iron species leached from MBC provided sufficient electron acceptors to stimulate DIR activity, thereby promoting IET among microorganisms. This result is consistent with the observed dissolution behavior of Fe(II) (Fig. 2a). These findings led to the conclusion that MBC significantly alters microbial community structure in suspension and promotes DIRB enrichment by leaching iron species from MBC.

Methanobacterium, *Methanothrix*, and *Methanosarcina* were the predominant methanogens in the suspension of all sample groups during the first 20 days (Fig. 5b). On the 30th day, the predominant genera in R2 and R3 were significantly altered compared with those in R1. Specifically, *Methanobacterium*, as a hydrogenotrophic methanogen [14], decreased from 37.4% to 44.9–19.3% and 17.4% in R2 and R3, respectively. In contrast, *Candidatus* Methanofastidiosum was significantly enriched in R2 and R3. *Candidatus* Methanofastidiosum has been reported as a methylotrophic methanogen that competes with hydrogenotrophic methanogens, and it may be more advantageous at low hydrogen partial pressure [70]. In addition, on Day 30, *Methanothrix* accounted for 27.1%, 32.2%, and 32.1% of the genera found in R1, R2, and R3, respectively. Although the relative abundances of *Methanothrix* did not show a noticeable difference in either R2 or R3, an increasing trend in R3 was evident with the occurrence of secondary mineralization, while R2 showed a decreasing trend. These findings suggest that Fe(II) accumulation, mediated by the leaching of iron species, stimulated secondary mineralization reactions, during which the released electrons were used by *Methanothrix*, thereby facilitating its enrichment. Meanwhile, *Methanothrix* is known as the acetoclastic methanogen and is capable of DIET [29]. Therefore, the iron species leached from MBC might enable suspension to cultivate functional microorganisms for the establishment and facilitation of DIET among the syntrophic partners involved in the degradation and methanation of OM.

3.4.4. Structures of microbial communities in biofilm

Firmicutes, Bacteroidota, and Chloroflexota were also the dominant phyla in biofilm (Fig. 5c). Thermodesulfobacteriota, as a bacterium capable of DIR [71], were significantly enriched in biofilm, especially in R3. An increased abundance of Thermodesulfobacteriota was observed with the addition of Fenton sludge in AD, verifying the occurrence of DIR [72]. *Romboutsia* in R3 was higher than that in R2 (Fig. 5d). Meanwhile, *Geobacter* reached 2.5% in R3 on Day 20, but its abundance in both the suspension and biofilm of biochar was lower (<0.3%). These results indicate that MBC can provide a favorable growth environment for DIRB, possibly because of the energetic advantage associated with Fe(III) reduction [73]. As for the archaeal communities in biofilm, *Methanobacterium*, *Methanothrix*, and *Methanosarcina* were the dominant archaeal genera in the biofilms of R2 and R3 (Fig. 5d). In particular, *Methanothrix* also increased progressively with the leaching of iron species in R3 and was significantly higher than that in R2 on Day 30. These observations further highlight the pivotal role of *Methanothrix* in anaerobic methanogenesis

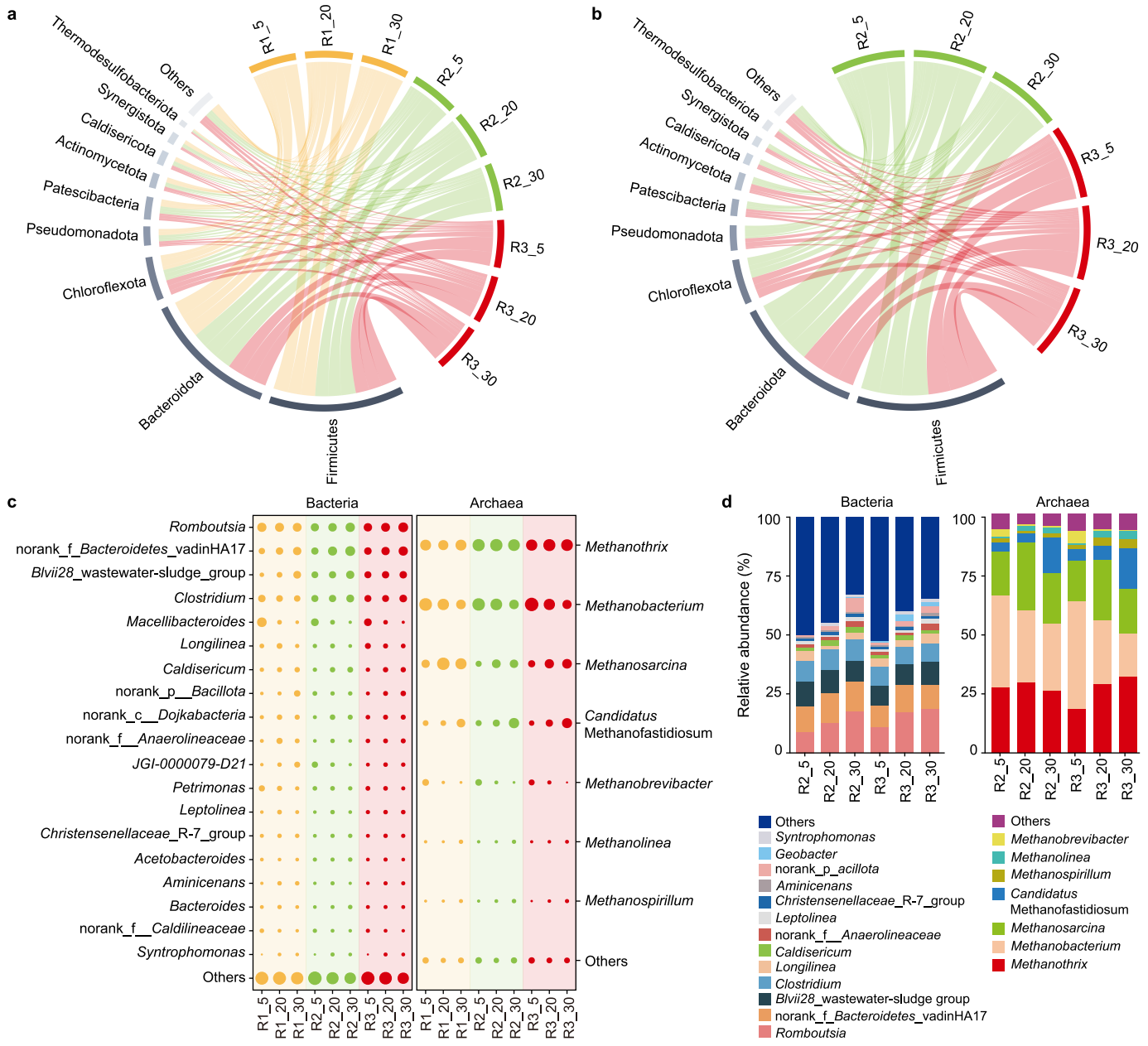

Fig. 5. **a**–**b**, The structures of bacterial communities at the phylum level: suspension (**a**) and biofilm (**b**). **c**–**d**, The structures of bacterial and archaeal communities at the genus level: suspension (**c**) and biofilm (**d**). R1: control group, R2: biochar group, and R3: magnetic biochar group. The number after the group represents the days: 5 (Day 5), 20 (Day 20), and 30 (Day 30).

mediated by the Fe(III)/Fe(II) redox cycle [29]. In particular, DIET was initially observed in *Geobacter* co-culture systems, occurring via conductive nanostructures composed of CytCs (e.g., *OmcS* and *OmcZ*) [74,75]. Meanwhile, *Geobacter* can function as a DIET partner of *Methanothrix* [14,29,76]. Thus, the biofilm formed on MBC might establish and promote DIET between electroactive genera (including *Geobacter* and *Romboutsia*) and methanogens (especially *Methanothrix*) under iron redox cycling mediated by the leaching of iron species. The upshot of all these is methanation promotion.

3.4.5. Changes in metabolic pathways for acidogenesis and methanogenesis

The iron species leached from MBC exerted a stimulatory effect on the key functional enzymes and metabolic pathways associated with acidogenesis and methanogenesis (Fig. 6). During acidogenesis, small-molecule OM are progressively converted into SCFAs via multistep enzymatic reactions accompanied by extracellular electron release [77]. Compared with R1 and R2, R3 exhibited markedly elevated abundances of pyruvate kinase (EC 2.7.1.40), pyruvate ferredoxin oxidoreductase (EC 1.2.7.8), acetaldehyde dehydrogenase (EC 1.2.1.10), and aldehyde dehydrogenase (EC 1.2.1.3) following the leaching of iron species. This result indicates that the iron species leached from MBC enhanced OM conversion and extracellular electron release by stimulating glycolysis, pyruvate metabolism, and acetogenesis pathways. Furthermore, in combination with the observed changes in iron ion concentrations in the liquid phase (Fig. 2a), Fe(III) leached from

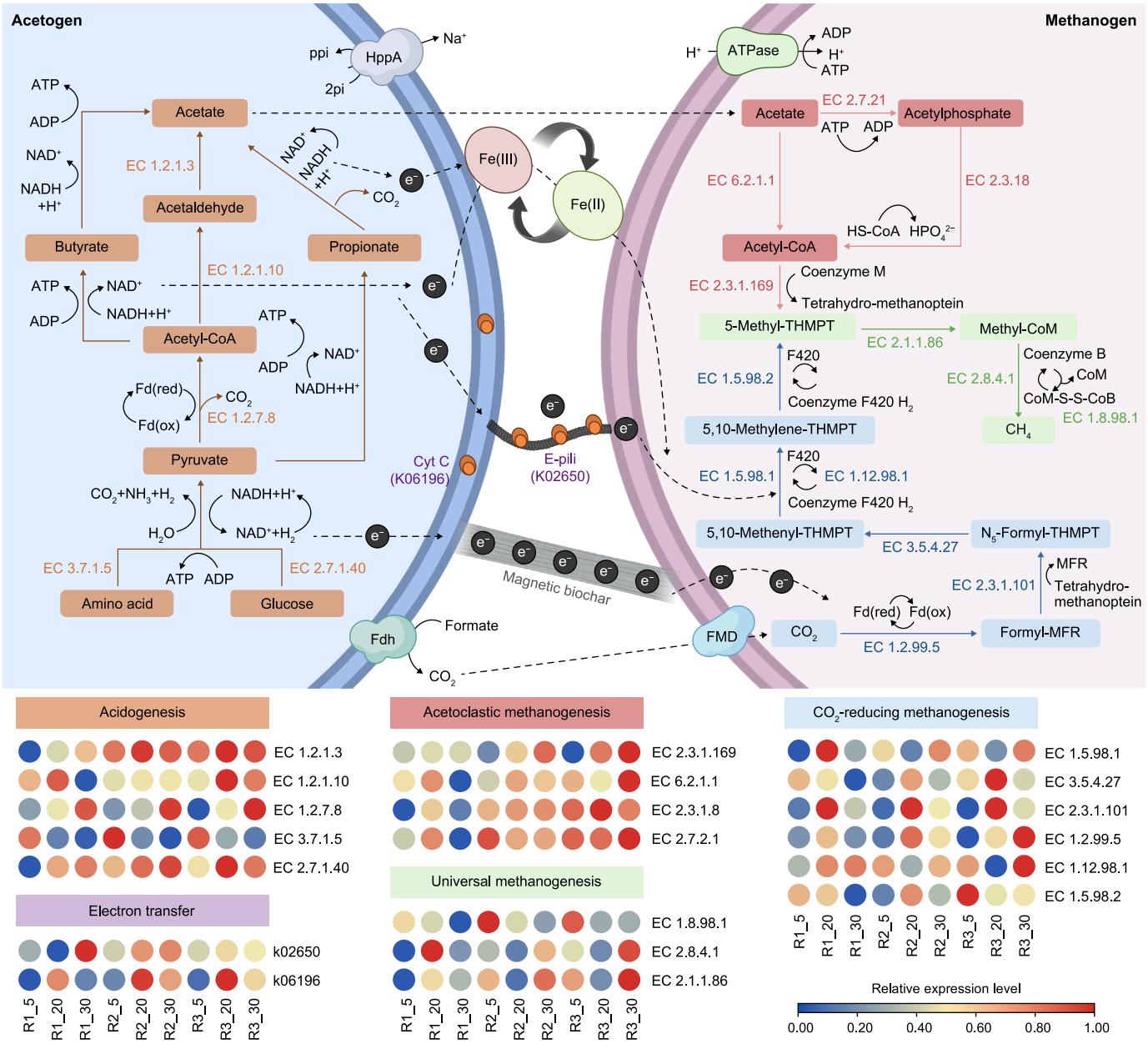

Fig. 6. Electron transfer modes and key enzymes during anaerobic digestion. The upper panel summarizes electron transfer pathways between electroactive bacteria and methanogens, and the lower panel highlights representative enzymes involved in acidogenesis and methanogenesis. R1: control group, R2: biochar group, R3: magnetic biochar group, Cyt C: cytochrome *c*, e-pili: electrically conductive pili, Fdh: formate dehydrogenase, FMD: formylmethanofuran dehydrogenase, MFR: methanofuran, CoM: coenzyme M, and THMPT: tetrahydromethanopterin. The dashed arrows mainly indicate the pathways of extracellular electron transfer (EET) and the flux of metabolites. EC 1.8.98.1 and EC 1.12.98.1 are involved in the regeneration processes of Coenzyme B and Coenzyme F420, respectively. The number after the group represents the days: 5 (Day 5), 20 (Day 20), and 30 (Day 30). Text colors in the upper panel match the color coding of the boxes in the lower panel, which indicate the corresponding metabolic pathways. Created with BioRender.

MBC could act as an electron acceptor for the electrons released during this process, thereby facilitating the iron redox cycle and modulating the syntrophic interactions between acetogens and methanogens. The presence of E-pili and CytCs (e.g., OmcS) served as essential components in DIET, with the corresponding synthesis proteins identified, suggesting the formation of a DIET-based methanogenic pathway. Although the abundance of type IV pili assembly protein PilA increased with the leaching of iron species in R3, it remained lower than that in R1 and R2. This may be because of a shift in the DIET pathway associated with methanogenesis. In contrast, the abundance of CytCs biosynthesis proteins in R3 gradually increased with the leaching of iron species during the first 20 days, followed by a decline on day 30. This trend was consistent with the observed CytCs activity (Fig. 4d). Interestingly, the abundance of enzymes associated with glycolysis and acetogenesis pathways also peaked on Day 20 in R3. These results imply that the intracellular electrons and adenosine triphosphate produced through glycolysis and acetogenesis in acetogens could be transferred to the cell membrane via CytCs during the first 20 days, facilitating electron transfer between the cells and MBC. With secondary mineralization stimulated by Fe(II) accumulation and the generation of new iron species (e.g., magnetite), the function of CytCs may be gradually replaced, leading to a subsequent decline in its abundance and activity [29].

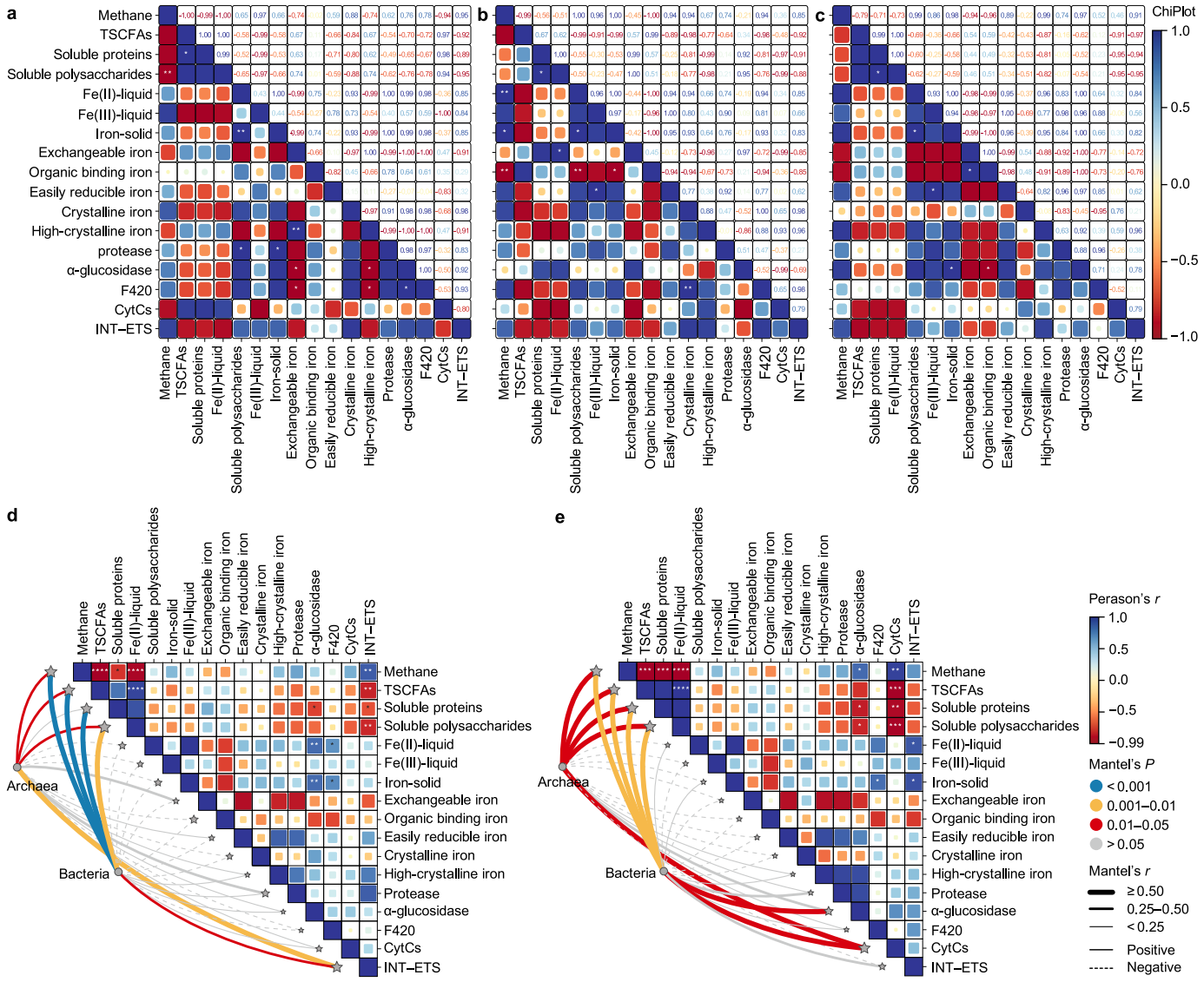

Fig. 7. **a**–**c**, Correlation analysis between anaerobic digestion performance and key operational parameters in different groups: control (**a**), biochar (**b**), and magnetic biochar group (**c**). **d**–**e**, Mantel test evaluating the relationship between microbial community and key operational parameters: archaea and bacteria in suspension (**d**) and biofilm (**e**). $*P < 0.05$, $**P < 0.01$, and $***P < 0.001$. TSCFAs: total short-chain fatty acids, CytCs: c-type cytochromes, and INT–ETS: iodinitrotetrazolium chloride–electron transport system.

During the methanogenesis stage, methanogens can either directly convert acetate into methane or reduce CO_2 to methane using the electrons released by syntrophic bacteria [14,29]. In the acetoclastic methanogenesis pathway, the abundances of acetate kinase (EC 2.7.2.1), phosphate acetyltransferase (EC 2.3.1.8), acetate-CoA ligase (EC 6.2.1.1), and acetyl-CoA synthase (EC 2.3.1.169) that could synergistically transform acetate into a methane precursor (5-Methyl-THMPT) were exceptionally enhanced in R3 on Day 30. As reported, *Methanothrix* can use acetyl-CoA to produce methane while also maintaining its proliferation within a microbial community [78], consistent with the microbial succession observed in this work. These results suggest that the leaching of iron species from MBC upregulates the expression of acetate kinase, phosphate acetyltransferase, acetate–CoA ligase, and acetyl–CoA synthase, thereby enhancing the conversion of acetate into methane. In addition, on Day 30, the essential enzymes associated with CO_2-reducing methanogenesis, including formylmethanofuran dehydrogenase (EC 1.2.99.5) and coenzyme F420 hydrogenase (EC 1.12.98.1), as well as the universal methanogenesis pathway, like tetrahydromethanopterin S-methyltransferase (EC 2.1.1.86) and coenzyme-B sulfoethylthiotransferase (EC 2.8.4.1), were significantly upregulated in R3. This phenomenon was closely associated with the Fe(III)/Fe(II) redox cycling mediated by the iron species leached from MBC. Specifically, Fe(III) leached from MBC can serve as an electron acceptor for acetogens, thereby ensuring a sustained supply of Fe(II) in AD. On Day 30, the proportion of Fe(II) in the solid phase began to decrease gradually, accompanied by a significant occurrence of secondary mineralization reaction (Fig. 2c and d). The electrons released during these reactions could be directly transferred by syntrophic microbes [29], thus facilitating CO_2-reducing methanogenesis. Overall, the iron species leached from MBC could establish a robust DIET pathway via Fe(III)/Fe(II) redox cycling, which selectively stimulated glycolysis, acetogenesis, and methanogenesis, including acetoclastic and CO_2-reducing methanation. With the generation of new iron species, DIET initially mediated by CytCs and MBC became predominantly driven by Fe(III)/Fe(II) redox cycling in conjunction with MBC.

3.5. Role of iron species leached from MBC during methanogenesis

A correlation-based analysis was conducted to explore the potential relationships among digester performance, iron species, and microbial community structures (Fig. 7; Supplementary Fig. S5). Compared with R1 and R2, R3 exhibited a strong negative correlation between Fe(II) in the liquid phase and intermediate metabolites, along with a notably strong positive correlation with the activities of hydrolytic enzymes (Fig. 7a–c). These findings suggest that the DIR mediated by iron species leached from MBC effectively promoted the conversion of intermediates (e.g., soluble polysaccharides, soluble proteins, and SCFAs) and facilitated electron release. Furthermore, strong correlations between Fe(II) in the liquid phase and iron minerals with varying degrees of crystallinity were observed in R3. Fe(II) in the liquid phase was negatively correlated with exchangeable, organic-bound, and crystalline iron but positively correlated with easily reducible and high-crystalline iron fractions. Meanwhile, from the perspective of time evolution (Supplementary Fig. S5), the shift in correlation to positive indicated that Fe(II) from MBC promoted the secondary mineralization of unstable iron minerals, establishing effective Fe(III)/Fe(II) redox cycling in AD. INT–ETS has been extensively used as an indicator of microbial electron transport activity [20]. Coenzyme F420 can accept electrons from the methanogenic respiratory chain to form $F420H_2$ (Fig. 6), which can serve as a key electron carrier that confers reductive power for methanogenesis [47]. In R3, both the concentrations of high-crystalline iron and Fe(II) in the liquid phase exhibited strong positive correlations with coenzyme F420 and INT–ETS. They confirmed the observed enrichment of electroactive microorganisms and secretion of electroactive substances (Fig. 4c and 5). In addition, high-crystalline iron was negatively correlated with F420 and INT–ETS on Day 5, but this shifted to a positive correlation on Day 20 (Supplementary Fig. S5). This result further confirmed that secondary mineralization mediated by Fe(II) accumulation enhanced IET efficiency. Therefore, the electron flux generated by Fe(III)/Fe(II) redox cycling is pivotal in facilitating DIET networks.

The Mantel test further illuminated the relationships between microbial communities in suspension and biofilm and AD performance parameters (Fig. 7d and e). A significant positive correlation was evident between both bacterial and archaeal communities in suspension and INT–ETS ($P < 0.01$), as well as between bacterial and archaeal communities in biofilms and CytCs ($P < 0.01$). These results provide further evidence that the electrons generated via Fe(III)/Fe(II) redox cycling mediated by the iron species leached from MBC are effectively shuttled among syntrophic microorganisms, thus reinforcing the development of a robust DIET pathway.

3.6. Overall understanding of iron species in MBC during AD

The mechanism by which the iron species leached from MBC promote methanogenesis is schematically illustrated in Fig. 8. During the hydrolysis stage, the Fe(III) species on MBC were rapidly leached into the liquid phase, thereby significantly increasing the Fe(II) concentration in this phase. This change was closely associated with the enrichment of DIRB (e.g., *Romboutsia* and *Clostridium*) in both suspension and biofilm. The leaching of Fe(III) species provided essential electron acceptors for DIR, which enhanced the hydrolysis of soluble proteins and polysaccharides and the release of extracellular electrons. These electrons were partially recycled via the Fe(III)/Fe(II) redox cycle and partially channeled through the DIET network across syntrophic microorganisms. During acidogenesis, the Fe(III) species-mediated iron redox cycling was tightly coupled with the degradation of SCFAs. In particular, the sustained Fe(II) accumulation in the liquid phase and the generation of crystalline iron species indicated an enhancement of the Fe(III)/Fe(II) redox cycling and sustained robust electron flow. This process further stimulated the enrichment of syntrophic microorganisms (e.g., norank_f__*Bacteroidetes*_vadinHA17 and *Geobacter*) in both suspension and biofilm, as well as the secretion of redox-active metabolites (e.g., CytCs), thereby improving the degradation SCFAs, particularly acetate and propionate. These outcomes find further support from the enhancement of glycolysis, pyruvate metabolism, and acetogenesis pathways. As methanogenesis occurred, the continued OM degradation drove the release of Fe(III) species from organic-bound iron and provided additional adsorption sites for Fe(II) adsorption. The coupling of this process with Fe(II) accumulation mediated by the leaching of iron species advanced secondary mineralization reaction, accompanied by the generation of high-crystalline iron species. The burst of electrons from this process significantly enhanced both acetoclastic and CO_2-reducing methanogenesis pathways, corresponding with a notable enrichment of *Methanothrix* in suspension and biofilm. The improved electrochemical properties, along with the increased activity of INT–ETS and coenzyme F420, confirmed the reinforcement of DIET. Simultaneously, this shift reduced the reliance on the CytC-mediated electron transfer pathway, indicating a transition in the DIET mechanism to one predominantly driven by the Fe(III)/Fe(II) redox cycle and conductive properties of MBC.

Overall, Fe(III) species on MBC are inevitably leached into the liquid phase during AD. The sustained Fe(III)/Fe(II) redox reaction triggered by the coupling of DIR and secondary mineralization results in a gradual transfer of leached Fe(III) into the solid phase, which is accompanied by a shift in Fe(III). This study identified the mechanism by which iron species leaching from MBC are promoted during AD by investigating the interactions between the dynamic behaviors of these species and biological reactions in AD. In particular, the Fe(III)/Fe(II) redox reaction provided sufficient precursors for the methanogenesis stage by inducing OM conversion and improving the efficiency of IET among syntrophic microorganisms by releasing a powerful electron flow, thereby promoting methanogenesis. From an economic standpoint, biochar and iron offer considerable cost advantages, with market prices ranging from USD0.08 to USD0.12 per kilogram [79]. The strategy of adding biochar increases methane accumulation by 37.0%, with an average of 465–543 mL per g VSS, and this increase translates into a net profit of approximately USD9.99 million [80]. Although the methane accumulation in the present study increased by 17.0% (305.3 mL per g VSS) with the addition of MBC, the moderate temperature operating conditions (35 °C) applied reduced operating costs to levels lower than those incurred under the high temperature operating conditions (55 °C) adopted in the previously cited work. Moreover, compared with WAS, food waste has more complex characteristics that necessitate additional pretreatment measures (e.g., sorting and homogenization), which inevitably increases investment in equipment [81]. Notably, the amount of MBC added was reduced by 50% compared with the aforementioned study. Furthermore, the excellent recyclability and superior reinforcement of MBC have been reported previously [14,82], further reducing the additional cost of dosing MBC. Nevertheless, the leaching of iron species simultaneously stimulated the iron loss effect of MBC, which inevitably weakened the strengthening effect of MBC as a conductive material [12]. On the basis of our findings, the rate of iron loss from MBC was 4.2% at the end of methanogenesis. Future studies should therefore evaluate

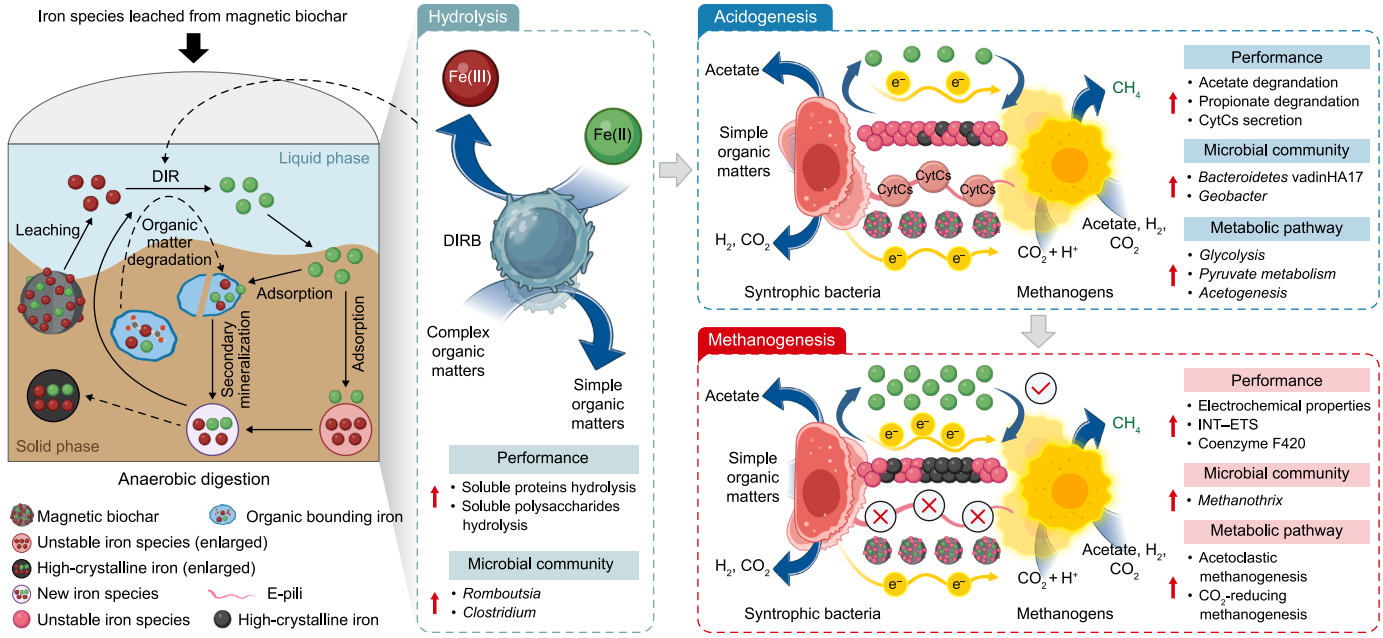

Fig. 8. Proposed mechanisms for iron species leached from magnetic biochar during anaerobic digestion. DIR: dissimilatory iron reduction, DIRB: dissimilatory iron-reducing bacteria, Cyt C: cytochrome *c*, e-pili: electrically conductive pili, and INT–ETS: iodinitrotetrazolium chloride–electron transport system. Solid arrows represent the migration and transformation of iron ions, dashed arrows represent the transition of iron oxides. Created with BioRender.

the interaction between the iron loss characteristics of MBC and the leaching of iron species during AD through MBC recycling. More importantly, the economic implications of iron loss in MBC should be analyzed from a life-cycle sustainability perspective, providing a theoretical basis and technical support for its engineering application.

4. Conclusion

This study aimed to uncover the mechanism by which the leaching of iron species from MBC enhances methane production during AD. Such species favorably influenced AD performance, with cumulative methane production in R3 increasing by 17.0% and 12.3% relative to R1 and R2, respectively. Initially, Fe(III) was leached from MBC into the liquid phase, driving a continuous increase in Fe(II) concentrations, with markedly higher Fe(II) levels in R3 than in R1 and R2. Concurrently, the content of organic-bound iron in R3 decreased with the leaching of Fe(III) species, whereas the concentration of high-crystalline iron increased. Correspondingly, the electrochemical properties and key enzymatic activities in R3 exhibited promotive effects. Microbial analysis revealed the selective enrichment of electroactive genera in suspension and biofilms, including *Romboutsia*, *Clostridium*, *Geobacter*, and *Methanothrix*, stimulating metabolic pathways such as glycolysis, pyruvate fermentation, acetogenesis, acetoclastic fermentation, and CO_2 reduction. Therefore, Fe(III) leaching improved hydrolysis, acidogenesis, and methanogenesis by establishing a stable Fe(III)/Fe(II) redox cycling network. Notably, the generation of stable Fe(III) species, mediated by secondary mineralization, reduced dependence on the CytCs-mediated electron-transfer pathway. It enabled a transition in the DIET pathway toward one primarily driven by Fe(III)/Fe(II) redox cycling and the conductive properties of MBC. Although the Fe(III) species leached from MBC exhibited strengthening properties, the rate of iron loss from MBC was 4.2% at the end of the methanogenesis stage, which diminished the strengthening effect of MBC as a conductive material. Future studies should therefore examine the trade-offs between the iron-loss characteristics of MBC and the leaching of iron species during AD, using recycled MBC to better adapt to an AD system. This would provide a theoretical basis and technical support for the sustainable waste management policies.

CRediT authorship contribution statement

Qing-Bin Meng: Writing - Original Draft, Visualization, Validation, Methodology, Investigation, Formal Analysis, Data Curation. **Zhang-Wei He:** Writing - Review & Editing, Writing - Original Draft, Supervision, Resources, Funding Acquisition, Conceptualization. **Zhi-Hua Li:** Resources, Project Administration, Investigation. **Cong-Cong Tang:** Resources, Methodology, Formal analysis, Writing - Review & Editing. **Ai-Juan Zhou:** Validation, Resources, Investigation. **Bin Liang:** Writing - Review & Editing, Visualization, Software. **Wenzong Liu:** Writing - Review & Editing, Resources, Investigation. **Yong-Xiang Ren:** Resources, Methodology, Investigation. **Aijie Wang:** Supervision, Funding Acquisition, Writing - Review & Editing.

Declaration of competing interest

The authors declare that they have no known competing financial interests or personal relationships that could have appeared to influence the work reported in this paper.

Dr. Aijie Wang, the Executive Editor of Environmental Science and Ecotechnology, was not involved in the editorial review or the decision to publish this article.

Acknowledgements

This work was supported by the National Natural Science Foundation of China (No. 52270139) and the State Key Laboratory of Urban-rural Water Resource and Environment (Grant No. HC202459).

Appendix A. Supplementary data

Supplementary data to this article can be found online at https://doi.org/10.1016/j.ese.2026.100660.

References

[1] M.C.M. Van Loosdrecht, D. Brdjanovic, Anticipating the next century of wastewater treatment, Science 344 (6191) (2014) 1452–1453, https://doi.org/10.1126/science.1255183.

[2] F. Xiong, Z. Su, Y. Tang, T. Dai, D. Wen, Global WWTP microbiome-based integrative information platform: from experience to intelligence, Environ. Sci. Ecotechnol. 20 (2024) 100370, https://doi.org/10.1016/j.ese.2023.100370.

[3] G.-J. Xie, B.-F. Liu, Q. Wang, J. Ding, N.-Q. Ren, Ultrasonic waste activated sludge disintegration for recovering multiple nutrients for biofuel production, Water Res. 93 (2016) 56–64, https://doi.org/10.1016/j.watres.2016.02.012.

[4] F. Wang, W. Huang, J. Chen, Y. Luo, J. Cao, F. Fang, X. Liu, Y. Wu, J. Luo, Non-antibiotic disinfectant synchronously interferes methane production and antibiotic resistance genes propagation during sludge anaerobic digestion: activation of microbial adaptation and reconfiguration of bacteria-archaea synergies, Water Res. 268 (2025) 122773, https://doi.org/10.1016/j.watres.2024.122773.

[5] H. He, X. Xin, W. Qiu, D. Li, Z. Liu, J. Ma, Waste sludge disintegration, methanogenesis and final disposal via various pretreatments: comparison of performance and effectiveness, Environ. Sci. Ecotechnol. 8 (2021) 100132, https://doi.org/10.1016/j.ese.2021.100132.

[6] H.-Y. Jin, Y.-X. Ren, C.-C. Tang, S. Zhang, J. Wang, A.-J. Zhou, B. Liang, W. Liu, A. Wang, Z.-W. He, Deciphering the synergistic effects and mechanisms of biochar and magnetite contained in magnetic biochar for enhancing methane production in anaerobic digestion of waste activated sludge, Water Res. (2025) 123734, https://doi.org/10.1016/j.watres.2025.123734.

[7] H. Li, L. You, H. Du, B. Yu, L. Lu, B. Zheng, Q. Zhang, K. He, N. Ren, Methane and nitrous oxide emissions from municipal wastewater treatment plants in China: a plant-level and technology-specific study, Environ. Sci. Ecotechnol. 20 (2024) 100345, https://doi.org/10.1016/j.ese.2023.100345.

[8] Y. Huang, K. Igarashi, L. Liu, D. Mayumi, T. Ujiie, L. Fu, M. Yang, Y. Lu, L. Cheng, S. Kato, M.K. Nobu, Methanol transfer supports metabolic syntrophy between bacteria and archaea, Nature 639 (8053) (2025) 190–195, https://doi.org/10.1038/s41586-024-08491-w.

[9] D.R. Lovley, Reach out and touch someone: potential impact of DIET (direct interspecies energy transfer) on anaerobic biogeochemistry, bioremediation, and bioenergy, Rev. Environ. Sci. Biotechnol. 10 (2) (2011) 101–105, https://doi.org/10.1007/s11157-011-9236-9.

[10] Y. Jing, J. Wan, I. Angelidaki, S. Zhang, G. Luo, iTRAQ quantitative proteomic analysis reveals the pathways for methanation of propionate facilitated by magnetite, Water Res. 108 (1) (2017) 212–221, https://doi.org/10.1016/j.watres.2016.10.077.

[11] C. Cruz Viggi, S. Rossetti, S. Fazi, P. Paiano, M. Majone, F. Aulenta, Magnetite particles triggering a faster and more robust syntrophic pathway of methanogenic propionate degradation, Environ. Sci. Technol. 48 (13) (2014) 7536–7543, https://doi.org/10.1021/es5016789.

[12] H. Geng, Y. Xu, R. Liu, D. Yang, X. Dai, Magnetic porous microspheres enhancing the anaerobic digestion of sewage sludge: synergistic free and attached methanogenic consortia, Water Res. 254 (1) (2024) 121393, https://doi.org/10.1016/j.watres.2024.121393.

[13] L. Hassanpourmoghadam, B. Aminzadeh Goharrizi, A. Torabian, E. Bouteh, B.E. Rittmann, Effect of Fe_3O_4 nanoparticles on anaerobic digestion of municipal wastewater sludge, Bioresour. Technol. 169 (2023) 106692, https://doi.org/10.1016/j.biombioe.2022.106692.

[14] H.-Y. Jin, Y.-X. Ren, C.-C. Tang, A.-J. Zhou, W. Liu, Z. Li, A. Wang, Z.-W. He, Biomethane production enhancement from waste activated sludge with recycled magnetic biochar: insights into the recycled strategies and mechanisms, J. Clean. Prod. 434 (2024) 139835, https://doi.org/10.1016/j.jclepro.2023.139835.

[15] H.-Y. Jin, Z.-W. He, Y.-X. Ren, C.-C. Tang, A.-J. Zhou, W. Liu, B. Liang, Z.-H. Li, A. Wang, Current advances and challenges for direct interspecies electron transfer in anaerobic digestion of waste activated sludge, Chem. Eng. J. 450 (2022) 137973, https://doi.org/10.1016/j.cej.2022.137973.

[16] H.-Y. Jin, Z.-W. He, Y.-X. Ren, C.-C. Tang, A.-J. Zhou, F. Chen, B. Liang, W. Liu, A. Wang, Role and significance of co-additive of biochar and nano-magnetite on methane production from waste activated sludge: non-synergistic rather than synergistic effects, Chem. Eng. J. 439 (2022) 135746, https://doi.org/10.1016/j.cej.2022.135746.

[17] D. Zhao, L. Ding, X. Wang, Q. Li, F. Zan, Y.-Y. Li, R. Chen, Deciphering the role of biochar pseudocapacitance strengthening in promoting syntrophic methanogenesis: microbial capacitance-tropism in propionate metabolism, Chem. Eng. J. 502 (2024) 158024, https://doi.org/10.1016/j.cej.2024.158024.

[18] L. Feng, H. Mu, Z. Gao, T. Hu, S. He, Y. Liu, S. You, Q. Zhao, L. Wei, Comprehensive insights into the impact of magnetic biochar on protein hydrolysis in sludge anaerobic digestion: protein structures, microbial activities and syntrophic metabolisms, Water Res. 260 (15) (2024) 121963, https://doi.org/10.1016/j.watres.2024.121963.

[19] L. Li, H. Liu, Y. Chen, D. Yang, C. Cai, S. Yuan, X. Dai, Effect of Magnet-Fe_3O_4 composite structure on methane production during anaerobic sludge digestion: establishment of direct interspecies electron transfer, Renew. Energy 188 (2022) 52–60, https://doi.org/10.1016/j.renene.2022.01.101.

[20] H.-Y. Jin, L. Yang, Y.-X. Ren, C.-C. Tang, A.-J. Zhou, W. Liu, Z. Li, A. Wang, Z.-W. He, Insights into the roles and mechanisms of a green-prepared magnetic biochar in anaerobic digestion of waste activated sludge, Sci. Total Environ. 896 (20) (2023) 165170, https://doi.org/10.1016/j.scitotenv.2023.165170.

[21] X. Yang, X. Tian, Y. Xue, C. Wang, Application of iron-modified biochar in the fields of adsorption and degradation of antibiotics, J. Environ. Manag. 380 (2025) 124875, https://doi.org/10.1016/j.jenvman.2025.124875.

[22] Y. Su, Y. Chen, J. Wu, Methane production from propionate enhanced by Met@Fe_3O_4 via increasing microbe–material attachment in a direct interspecies electron-transfer process, ACS Sustain. Chem. Eng. 9 (1) (2021) 471–480, https://doi.org/10.1021/acssuschemeng.0c07652.

[23] L. Feng, Z. Gao, T. Hu, S. He, Y. Liu, J. Jiang, Q. Zhao, L. Wei, A review of application of combined biochar and iron-based materials in anaerobic digestion for enhancing biogas productivity: mechanisms, approaches and performance, Environ. Res. 234 (1) (2023) 116589, https://doi.org/10.1016/j.envres.2023.116589.

[24] C.M. Hansel, S.G. Benner, S. Fendorf, Competing Fe(II)-induced mineralization pathways of ferrihydrite, Environ. Sci. Technol. 39 (18) (2005) 7147–7153, https://doi.org/10.1021/es050666z.

[25] A. Kappler, C. Bryce, M. Mansor, U. Lueder, J.M. Byrne, E.D. Swanner, An evolving view on biogeochemical cycling of iron, Nat. Rev. Microbiol. 19 (6) (2021) 360–374, https://doi.org/10.1038/s41579-020-00502-7.

[26] E.D. Melton, E.D. Swanner, S. Behrens, C. Schmidt, A. Kappler, The interplay of microbially mediated and abiotic reactions in the biogeochemical Fe cycle, Nat. Rev. Microbiol. 12 (12) (2014) 797–808, https://doi.org/10.1038/nrmicro3347.

[27] S. Cui, R. Wang, Q. Chen, L. Pugliese, S. Wu, Geobatteries in environmental biogeochemistry: electron transfer and utilization, Environ. Sci. Ecotechnol. 22 (2024) 100446, https://doi.org/10.1016/j.ese.2024.100446.

[28] H. Xu, S. Hei, W. Fu, X. Zhang, P. Liang, B. Pan, X. Huang, Unraveling the trade-off effect of pyrogenic carbons between biopseudocapacitors and bioconductors during anaerobic methanogenesis, Environ. Sci. Technol. 59 (5) (2025) 2861–2874, https://doi.org/10.1021/acs.est.4c10638.

[29] H. Xu, M. Wang, S. Hei, X. Qi, X. Zhang, P. Liang, W. Fu, B. Pan, X. Huang, Neglected role of iron redox cycle in direct interspecies electron transfer in anaerobic methanogenesis: inspired from biogeochemical processes, Water Res. 262 (15) (2024) 122125, https://doi.org/10.1016/j.watres.2024.122125.

[30] G. Kor-Bicakci, C. Eskicioglu, Recent developments on thermal municipal sludge pretreatment technologies for enhanced anaerobic digestion, Renew. Sustain. Energy Rev. 110 (2019) 423–443, https://doi.org/10.1016/j.rser.2019.05.002.

[31] Q. Jiang, H. Liu, Y. Zhang, M.-h. Cui, B. Fu, H.-b. Liu, Insight into sludge anaerobic digestion with granular activated carbon addition: methanogenic acceleration and methane reduction relief, Bioresour. Technol. 319 (2021) 124131, https://doi.org/10.1016/j.biortech.2020.124131.

[32] Y. Shen, Y. Yu, Y. Zhang, M. Urgun-Demirtas, H. Yuan, N. Zhu, X. Dai, Role of redox-active biochar with distinctive electrochemical properties to promote methane production in anaerobic digestion of waste activated sludge, J. Clean. Prod. 278 (2021) 123212, https://doi.org/10.1016/j.jclepro.2020.123212.

[33] W. Hu, H.-Y. Jin, X.-Y. Gao, C.-C. Tang, A.-J. Zhou, W. Liu, Y.-X. Ren, Z. Li, Z.-W. He, Biochar derived from alkali-treated sludge residue regulates anaerobic digestion: enhancement performance and potential mechanisms, Environ. Res. 251 (2024) 118578, https://doi.org/10.1016/j.envres.2024.118578.

[34] C.-C. Tang, B.-C. Zhang, X.-Y. Yao, T. Sangeetha, A.-J. Zhou, W. Liu, Y.-X. Ren, Z. Li, A. Wang, Z.-W. He, Natural zeolite enhances anaerobic digestion of waste activated sludge: insights into the performance and the role of biofilm, J. Environ. Manag. 345 (2023) 118704, https://doi.org/10.1016/j.jenvman.2023.118704.

[35] H.-Y. Jin, X.-Y. Yao, C.-C. Tang, A.-J. Zhou, W. Liu, Y.-X. Ren, Z. Li, A. Wang, Z.-W. He, Magnetite modified zeolite as an alternative additive to promote methane production from anaerobic digestion of waste activated sludge, Renew. Energy 224 (2024) 120181, https://doi.org/10.1016/j.renene.2024.120181.

[36] R. Han, J. Lv, Z. Huang, S. Zhang, S. Zhang, Pathway for the production of hydroxyl radicals during the microbially mediated redox transformation of iron (Oxyhydr)oxides, Environ. Sci. Technol. 54 (2) (2020) 902–910, https://doi.org/10.1021/acs.est.9b06220.

[37] M. Wang, Z. Zhao, Y. Li, S. Liang, Y. Meng, T. Ren, X. Zhang, Y. Zhang, Control the greenhouse gas emission via mediating the dissimilatory iron reduction: fulvic acid inhibit secondary mineralization of ferrihydrite, Water Res. 218 (30) (2022) 118501, https://doi.org/10.1016/j.watres.2022.118501.

[38] Y. Sun, M. Wang, L. Liang, C. Sun, X. Wang, Z. Wang, Y. Zhang, Continuously feeding fenton sludge into anaerobic digesters: iron species change and operating stability, Water Res. 226 (1) (2022) 119283, https://doi.org/10.1016/j.watres.2022.119283.

[39] H.-Y. Yuan, L.-J. Ding, E.F. Zama, P.-P. Liu, W.N. Hozzein, Y.-G. Zhu, Biochar modulates methanogenesis through electron syntrophy of microorganisms with ethanol as a substrate, Environ. Sci. Technol. 52 (21) (2018) 12198–12207, https://doi.org/10.1021/acs.est.8b04121.

[40] P. Xie, Q.-S. Wang, W.-Y. Qu, X. Chen, Y.-J. Feng, J. Ma, N.-Q. Ren, S.-H. Ho, Revealing real impact of microalgae on seasonal dynamics of bacterial community in a pilot-scale microalgal-bacterial consortium system, Water Res. 274 (15) (2025) 123145, https://doi.org/10.1016/j.watres.2025.123145.
[41] Q. Yin, S. Yang, Z. Wang, L. Xing, G. Wu, Clarifying electron transfer and metagenomic analysis of microbial community in the methane production process with the addition of ferroferric oxide, Chem. Eng. J. 333 (2018) 216–225, https://doi.org/10.1016/j.cej.2017.09.160.
[42] Z.-W. He, W.-Z. Liu, Q. Gao, C.-C. Tang, L. Wang, Z.-C. Guo, A.-J. Zhou, A.-J. Wang, Potassium ferrate addition as an alternative pre-treatment to enhance short-chain fatty acids production from waste activated sludge, Bioresour. Technol. 247 (2018) 174–181, https://doi.org/10.1016/j.biortech.2017.09.073.
[43] T. Wang, D. Zhang, L. Dai, B. Dong, X. Dai, Magnetite triggering enhanced direct interspecies electron transfer: a scavenger for the blockage of electron transfer in anaerobic digestion of high-solids sewage sludge, Environ. Sci. Technol. 52 (12) (2018) 7160–7169, https://doi.org/10.1021/acs.est.8b00891.
[44] X. Zhang, J. Hou, S. Zhang, T. Cai, S. Liu, W. Hu, Q. Zhang, Standardization and micromechanistic study of tetracycline adsorption by biochar, Biochar 6 (1) (2024) 12, https://doi.org/10.1007/s42773-023-00299-7.
[45] A. Mumtaz, J. Iqbal, M. Mumtaz, M. Oneeb, Innovative hafnium oxide-vanadium oxide electrode with remarkably enhanced specific capacitance for supercapacitors, Energy 324 (2025) 136042, https://doi.org/10.1016/j.energy.2025.136042.
[46] X. Ji, J. Tang, J. Zhang, Effects of salt stress on the morphology, growth and physiological parameters of *Juglansmicrocarpa L.* seedlings, Plants 11 (18) (2022) 2381, https://doi.org/10.3390/plants11182381.
[47] Z. Shi, S. Campanaro, M. Usman, L. Treu, A. Basile, I. Angelidaki, S. Zhang, G. Luo, Genome-centric metatranscriptomics analysis reveals the role of hydrochar in anaerobic digestion of waste activated sludge, Environ. Sci. Technol. 55 (12) (2021) 8351–8361, https://doi.org/10.1021/acs.est.1c01995.
[48] M. Dorner, S. Behrens, Biochar as ammonia exchange biofilm carrier for enhanced aerobic nitrification in activated sludge, Bioresour. Technol. 413 (2024) 131374, https://doi.org/10.1016/j.biortech.2024.131374.
[49] Q. Sun, D. Li, Y. He, Q. Ping, L. Wang, Y. Li, Improved anaerobic digestion of waste activated sludge under ammonia stress by nanoscale zero-valent iron/peracetic acid pretreatment and hydrochar regulation: insights from multi-omics analyses, Water Res. (1) (2025) 123497, https://doi.org/10.1016/j.watres.2025.123497.
[50] F.A.M. De Bok, C.M. Plugge, A.J.M. Stams, Interspecies electron transfer in methanogenic propionate degrading consortia, Water Res. 38 (6) (2004) 1368–1375, https://doi.org/10.1016/j.watres.2003.11.028.
[51] Y. Su, L. Feng, X. Duan, H. Peng, Y. Zhao, Y. Chen, Deciphering the function of Fe_3O_4 in alleviating propionate inhibition during high-solids anaerobic digestion: insights of physiological response and energy conservation, Water Res. 270 (15) (2025) 122811, https://doi.org/10.1016/j.watres.2024.122811.
[52] Y. Wang, H. Wang, J.-S. He, X. Feng, Iron-mediated soil carbon response to water-table decline in an alpine wetland, Nat. Commun. 8 (1) (2017) 15972, https://doi.org/10.1038/ncomms15972.
[53] L. Liu, J. Li, L. Su, D. Fang, L. Zhou, An integrated process incorporating pH-controlled biomineralization and sulfate bioreduction to facilitate recovery of schwertmannite and sulfated polysaccharides from acid mine drainage, Chem. Eng. J. 487 (2024) 150614, https://doi.org/10.1016/j.cej.2024.150614.
[54] P. Wilfert, P.S. Kumar, L. Korving, G.-J. Witkamp, M.C.M. van Loosdrecht, The relevance of phosphorus and iron chemistry to the recovery of phosphorus from wastewater: a review, Environ. Sci. Technol. 49 (16) (2015) 9400–9414, https://doi.org/10.1021/acs.est.5b00150.
[55] X. Wang, Y. Chen, W. Ding, L. Wei, N. Shen, B. Bian, G. Wang, Y. Zhou, Organic binding iron formation and its mitigation in cation exchange resin assisted anaerobic digestion of chemically enhanced primary sedimentation sludge, Water Res. 247 (1) (2023) 120806, https://doi.org/10.1016/j.watres.2023.120806.
[56] Q. Wang, C. Zhang, D. Patel, H. Jung, P. Liu, B. Wan, S.G. Pavlostathis, Y. Tang, Coevolution of iron, phosphorus, and sulfur speciation during anaerobic digestion with hydrothermal pretreatment of sewage sludge, Environ. Sci. Technol. 54 (13) (2020) 8362–8372, https://doi.org/10.1021/acs.est.0c00501.
[57] T. Weber, T. Allard, E. Tipping, M.F. Benedetti, Modeling iron binding to organic matter, Environ. Sci. Technol. 40 (24) (2006) 7488–7493, https://doi.org/10.1021/es0607077.
[58] Y. Xu, Y. Lu, X. Dai, B. Dong, The influence of organic-binding metals on the biogas conversion of sewage sludge, Water Res. 126 (1) (2017) 329–341, https://doi.org/10.1016/j.watres.2017.09.046.
[59] S. Hu, H. Zhang, Y. Yang, W. Wang, W. Zhou, X. Shen, C. Liu, Reductive sequestration of Cr(VI) and immobilization of C during the microbially mediated transformation of ferrihydrite-Cr(VI)-fulvic acid coprecipitates, Environ. Sci. Technol. 57 (22) (2023) 8323–8334, https://doi.org/10.1021/acs.est.2c09803.
[60] K. Fricke, F. Harnisch, U. Schröder, On the use of cyclic voltammetry for the study of anodic electron transfer in microbial fuel cells, Energy Environ. Sci. 1 (1) (2008) 144–147, https://doi.org/10.1039/B802363H.
[61] N. Li, X. Quan, M. Zhuo, X. Zhang, Y. Quan, P. Liang, Enhancing methanogenesis of anaerobic granular sludge by incorporating Fe/Fe oxides nanoparticles aided with biofilm disassembly agents and mediating redox activity of extracellular polymer substances, Water Res. 216 (1) (2022) 118293, https://doi.org/10.1016/j.watres.2022.118293.
[62] J. Ye, A. Hu, G. Ren, M. Chen, J. Tang, P. Zhang, S. Zhou, Z. He, Enhancing sludge methanogenesis with improved redox activity of extracellular polymeric substances by hematite in red mud, Water Res. 134 (1) (2018) 54–62, https://doi.org/10.1016/j.watres.2018.01.062.
[63] S. Wang, S. Cheng, K. Zhang, F. Liu, R. Liu, X. Gao, J. Li, L. Du, Comparing the effects and mechanisms of granular activated carbon and magnetite nanoparticles in dry anaerobic digestion: focusing on microbial electron transfer and metagenomic evidence, Chem. Eng. J. 497 (2024) 155705, https://doi.org/10.1016/j.cej.2024.155705.
[64] L. Wang, Y. Wu, Z. You, H. Bao, L. Zhang, J. Wang, Electrochemical impedance spectroscopy (EIS) reveals the role of microbial fuel cell-ceramic membrane bioreactor (MFC-CMBR): electricity utilization and membrane fouling, Water Res. 222 (15) (2022) 118854, https://doi.org/10.1016/j.watres.2022.118854.
[65] S. Li, Y. Cao, C. Bi, Y. Zhang, Promoting electron transfer to enhance anaerobic treatment of azo dye wastewater with adding $Fe(OH)_3$, Bioresour. Technol. 245 (2017) 138–144, https://doi.org/10.1016/j.biortech.2017.08.066.
[66] X. Guo, J. Feng, Z. Shi, X. Zhou, M. Yuan, X. Tao, L. Hale, T. Yuan, J. Wang, Y. Qin, A. Zhou, Y. Fu, L. Wu, Z. He, J.D. Van Nostrand, D. Ning, X. Liu, Y. Luo, J.M. Tiedje, Y. Yang, J. Zhou, Climate warming leads to divergent succession of grassland microbial communities, Nat. Clim. Change 8 (9) (2018) 813–818, https://doi.org/10.1038/s41558-018-0254-2.
[67] M. Fincker, J.A. Huber, V.J. Orphan, M.S. Rappé, A. Teske, A.M. Spormann, Metabolic strategies of marine subseafloor chloroflexi inferred from genome reconstructions, Environ. Microbiol. 22 (8) (2020) 3188–3204, https://doi.org/10.1111/1462-2920.15061.
[68] H. Zhang, W. Li, C. Zhou, J. Zhang, Y. Pei, L. Zang, Comparison of cobalt ferrate-based nanoparticles for promoting biomethane evolution from lactic acid anaerobic digestion, Bioresour. Technol. 347 (2022) 126689, https://doi.org/10.1016/j.biortech.2022.126689.
[69] D. Lu, B. Xing, Y. Liu, Z. Wang, X. Xu, L. Zhu, Enhanced production of short-chain fatty acids from waste activated sludge by addition of magnetite under suitable alkaline condition, Bioresour. Technol. 289 (2019) 121713, https://doi.org/10.1016/j.biortech.2019.121713.
[70] M.K. Nobu, T. Narihiro, C. Rinke, Y. Kamagata, S.G. Tringe, T. Woyke, W.-T. Liu, Microbial dark matter ecogenomics reveals complex synergistic networks in a methanogenic bioreactor, ISME J. 9 (8) (2015) 1710–1722, https://doi.org/10.1038/ismej.2014.256.
[71] X. Wang, J. Zhang, Y. Xie, X. Li, J. Ran, M. Zhang, L. Zhang, A. Zhang, The effect of fenton sludge on anaerobic digestion of papermaking wastewater in an upflow anaerobic sludge blanket reactor, J. Environ. Manag. 370 (2024) 122762, https://doi.org/10.1016/j.jenvman.2024.122762.
[72] C. Wang, Y. Liu, S. Jin, H. Chen, X. Xu, Z. Wang, B. Xing, L. Zhu, Responsiveness extracellular electron transfer (EET) enhancement of anaerobic digestion system during start-up and starvation recovery stages via magnetite addition, Bioresour. Technol. 272 (2019) 162–170, https://doi.org/10.1016/j.biortech.2018.10.013.
[73] K.A. Weber, L.A. Achenbach, J.D. Coates, Microorganisms pumping iron: anaerobic microbial iron oxidation and reduction, Nat. Rev. Microbiol. 4 (10) (2006) 752–764, https://doi.org/10.1038/nrmicro1490.
[74] Z.M. Summers, H.E. Fogarty, C. Leang, A.E. Franks, N.S. Malvankar, D.R. Lovley, Direct exchange of electrons within aggregates of an evolved syntrophic coculture of anaerobic bacteria, Science 330 (6009) (2010) 1413–1415, https://doi.org/10.1126/science.1196526.
[75] Y. Gu, V. Srikanth, A.I. Salazar-Morales, R. Jain, J.P. O'Brien, S.M. Yi, R.K. Soni, F.A. Samatey, S.E. Yalcin, N.S. Malvankar, Structure of *Geobacter* pili reveals secretory rather than nanowire behaviour, Nature 597 (7876) (2021) 430–434, https://doi.org/10.1038/s41586-021-03857-w.
[76] Z. Zhao, Y. Zhang, Q. Yu, Y. Dang, Y. Li, X. Quan, Communities stimulated with ethanol to perform direct interspecies electron transfer for syntrophic metabolism of propionate and butyrate, Water Res. 102 (1) (2016) 475–484, https://doi.org/10.1016/j.watres.2016.07.005.
[77] G. You, C. Wang, P. Wang, J. Chen, Y. Gao, Y. Li, Y. Xu, Long-term transformation of nanoscale zero-valent iron explains its biological effects in anaerobic digestion: from ferroptosis-like death to magnetite-enhanced direct electron transfer networks, Water Res. 241 (1) (2023) 120115, https://doi.org/10.1016/j.watres.2023.120115.
[78] M. Zhang, Y. Han, Y. Zeng, T. Wang, Z. Wang, Y. Wu, N. Li, F.L. Lobo, X. Wang, Understanding the microbial processes on carbon brushes that accelerate methanogenesis of long-chain fatty acids in anaerobic digestion, Water Res. 273 (1) (2025) 123084, https://doi.org/10.1016/j.watres.2024.123084.
[79] J. Qian, S. Bai, L. Wu, M. Geng, G. Chen, F. Jiang, Energy recovery from corn straw-based biochar@MIL-88A(Fe)-mediated anaerobic digestion of waste activated sludge under norfloxacin: metabolism and antibiotic resistance gene fates, J. Environ. Sci. (2025), https://doi.org/10.1016/j.jes.2025.07.034.
[80] L. Zhang, E.Y. Lim, K.-C. Loh, Y.S. Ok, J.T.E. Lee, Y. Shen, C.-H. Wang, Y. Dai, Y.W. Tong, Biochar enhanced thermophilic anaerobic digestion of food waste: focusing on biochar particle size, microbial community analysis and pilot-scale application, Energy Convers. Manag. 209 (1) (2020) 112654, https://doi.org/10.1016/j.enconman.2020.112654.
[81] P. Chen, F. Xing, W. Li, E. Wang, Y. Zheng, X. Wu, B. Li, R. Dong, J. Guo, Deployment of temperature-specific thermal hydrolysis pretreatment in anaerobic co-digestion of sewage sludge and food waste could augment the economic benefits, Chem. Eng. J. 502 (2024) 157835, https://doi.org/10.1016/j.cej.2024.157835.